

Downlink Analysis of NOMA-enabled Cellular Networks with 3GPP-inspired User Ranking

Praful D. Mankar and Harpreet S. Dhillon

Abstract

This paper provides a comprehensive downlink analysis of non-orthogonal multiple access (NOMA) enabled cellular networks using tools from stochastic geometry. As a part of this analysis, we develop a novel 3GPP-inspired user ranking technique to construct a user cluster for the non-orthogonal transmission by grouping users from the cell center (CC) and cell edge (CE) regions. This technique allows to partition the users with distinct link qualities, which is imperative for the NOMA performance. Our analysis is focused on the performance of a user cluster in the *typical cell*, which is significantly different from the standard stochastic geometry-based approach of analyzing the performance of the *typical user*. For this setting, we first derive the moments of the meta distributions for the CC and CE users under NOMA and orthogonal multiple access (OMA). Using this, we then derive the distributions of the transmission rates and mean packet delays under non-real time (NRT) and real-time (RT) service models, respectively, for both CC and CE users. Finally, we study two resource allocation (RA) techniques with the objective of maximizing the cell sum rate (CSR) under NRT service, and the sum effective capacity (SEC) under RT service. In addition to providing several useful design insights, our results demonstrate that NOMA provides improved rate region and higher CSR as compared to OMA. In addition, we also show that NOMA provides better SEC as compared to OMA for the higher user density.

Index Terms

Non-orthogonal multiple access, user ranking, meta distribution, transmission rate, packet delay, cell sum rate, effective capacity, Poisson point process.

The authors are with Wireless@VT, Bradley Department of Electrical and Computer Engineering, Virginia Tech, Blacksburg, VA. Email: {prafuldm, hdhillon}@vt.edu. This paper will be presented in part at IEEE Globecom 2019 [1]. The support of the US National Science Foundation (Grant CNS-1814477) is gratefully acknowledged.

I. INTRODUCTION

Owing to its superior spectral efficiency, NOMA has emerged as a promising candidate for the future wireless cellular networks. Unlike traditional OMA, NOMA enables the BSs to concurrently serve multiple users using the same resource block (RB); see [2] and the references therein. In NOMA, the BS superimposes multiple layers of messages at different power levels and the user decodes its intended message using successive interference cancellation (SIC) technique. In particular, each user first decodes and cancels interference power from the layers assigned to the users with weaker channels successively using SIC and then decodes its own message. While the OMA ends up allocating most of the resources to the users with poor channel conditions in order to provide a certain level of quality of service (QoS), NOMA allows the BS to concurrently serve these weaker users by grouping them with the ones having better channel conditions so that the weaker users meet their QoS requirements without adversely affecting the performance of the stronger users. This naturally results in a higher cell ergodic capacity and a lower rate outage in case of NOMA [3].

A. Prior Art

The set of users scheduled for the non-orthogonal transmission in NOMA is often termed as the *user cluster*. In order to form a user cluster, one needs to first rank users based on their channel gains (both large-scale path losses and small-scale fading effects) and perceived inter-cell interference, and then place users with distinct link qualities in the same cluster [4]. However, since the prior works on NOMA are mostly focused on the single cell NOMA analysis, the users are ranked solely based on their distances from the BS [5], [6] or based on their link qualities [3], [7]–[9]. While such user ranking is meaningful in the context of single cell analysis, it ignores the impact of the inter cell interference which is crucial for accurate performance analysis of NOMA [10]. While stochastic geometry has emerged as a powerful tool to perform multi-cell analysis of cellular networks over the past decade [11]–[13], incorporating sophisticated user ranking based jointly on the link qualities and inter-cell interference is challenging. This is because of the correlation in the corresponding desired and inter-cell interference powers received by the users within the same cell. Therefore, most of the existing works in this direction ignore these correlations and instead rank the users in the order of their mean desired signal powers (i.e., link distances) so that the i -th closest user becomes the i -th strongest user. Within this general

direction, the authors of [14]–[18] analyzed N -ranked NOMA in cellular networks assuming that the BSs follow a PPP. In [18], the uplink success probability is derived assuming that the users follow a Poisson cluster process (PCP). In [14], the downlink success probability is derived while forming the user cluster within the indisk of the Poisson-Voronoi (PV) cell. However, this may underestimate the NOMA performance gains because users within the indisk of a PV cell will usually experience similar channel conditions and hence lack channel gain imbalance that results in the NOMA gains (see [4]). The moments of the *meta distribution* of the signal-to-interference ratio (SIR) [19] are derived for the downlink in [15], [16] and uplink in [16] by ranking the users based on their link distances. However, [16] ignores the joint decoding of the subset of layers associated with SIC. Nonetheless, considering the aforementioned distance-based user ranking technique, [15]–[18] derive the ordered distance distributions of the clustered users while assuming that their link distances follow the distance distribution of the typical link (in the network) independently of each other. As implied above already, this ignores the fact that the user location in a PV cell is a function of the BS point process. A key unintended consequence of this approach is that it does not necessarily confine the user cluster in a PV cell, which is a significant approximation of the underlying setup (see Fig. 1, Middle and Left). The spectral efficiency of the K -tier heterogeneous cellular networks is analyzed in [20] wherein the small cells serve their users using two-user NOMA with distance-based ranking. On similar lines, [21] derives the outage probability for two-user downlink NOMA cellular networks, modeled as a PPP, by ranking the users based on the channel gains normalized by their received inter-cell interference powers. The normalized gains are assumed to be independent and identically distributed (i.i.d.). However, this ignores the fact that the link distances or the inter-cell interference powers associated with the users within the PV cell are correlated as discussed above.

A more reasonable way of accurately ranking the users is to form a user cluster by selecting users from distinct regions of the PV cell. One way of constructing these regions is based on the ratio of mean powers (i.e., path-losses) received from the serving and dominant interfering BSs. In particular, a PV cell can be divided into the cell center (CC) region, wherein the ratio is above a threshold τ , and the cell edge (CE) region, wherein the ratio is below τ . A similar approach of classifying users as CC and CE is also used in 3GPP studies to analyze the performance of schemes such as soft frequency reuse (SFR) [22]. Inspired by this, we characterize the CC and CE users based on their path-losses from the serving and dominant interfering BSs to pair them

for the two-user NOMA system. While the proposed approach can be directly extended to the N -user NOMA using $N - 1$ region partitioning thresholds, we focus on the two-user NOMA for the ease of exposition. The proposed user pairing technique helps to construct the user cluster with distinct link qualities (which is essential for the NOMA performance [4]) because of two key reasons: 1) the order statistic of received powers at different users in the cell is dominated by the path-losses to those users [23], and 2) the dominant interfering BS contributes most of the interference power in the PPP setting [24].

Besides user ranking, RA is an integral part of the NOMA design. On these lines, the prior works have investigated RA for the downlink NOMA system using a variety of performance metrics, such as user fairness [8], [9], [25] and weighted sum rate maximization [9], [26], [27]. Further, in order to ensure certain level of QoS for downlink users, the RA problems for maximizing the sum rate [9], [14], [28] or the energy efficiency [9], [29], [30] subject to a minimum transmission rate constraint have also been investigated. In addition, [31] has demonstrated that the achievable sum rate in NOMA is always higher than that of the OMA under minimum transmission rate constraints when both techniques employ the optimal RA. While these formulations are meaningful for the full buffer NTR services, such as file downloading, they are not quite suitable for delay-sensitive applications with RT traffic, such as video streaming and augmented reality, which are becoming even more important in the context of emerging 5G networks. For such applications, it is important to consider RA formulations that explicitly consider delay constraints. In this context, the effective capacity, defined in [32] as the maximum achievable arrival rate that satisfy a delay QoS constraint, is analyzed for NOMA in [33]–[35] for the downlink case and in [36], [37] for the uplink case. However, in general, the existing works on the delay analysis of NOMA are relatively sparse. Besides, the aforementioned works on RA with the focus on sum rate [8], [9], [25], [28]–[31] and effective capacity [33]–[37] are limited to the single cell and hence do not capture the impact of inter-cell interference.

B. Contributions

The primary objective of this paper is to characterize the downlink performance of the CC and CE users in a NOMA-enabled cellular network under the 3GPP-inspired user ranking technique described above. From the stochastic geometry perspective, our approach focuses on the performance of the *typical cell*, which departs significantly from the standard approach of

analyzing the performance of the *typical user* in a cellular network that is selected independently of the BS locations. It is well-known that this typical user falls in the *Crofton cell* because of which it may not represent the performance of the users in the typical cell. Hence, we focus on the performance analysis of the typical CC and CE users contained in the typical cell of the network. For this setting, we analyze the link performance of the CC and CE users and also investigate the RA techniques for RT and NRT services. Key contributions of our analysis are briefly summarized below.

- 1) This paper presents a novel 3GPP-inspired user pairing technique for NOMA to accurately select the CC and CE users with distinct link qualities for the non-orthogonal transmission.
- 2) The moments of the meta distributions for the CC and CE users belonging to the typical cell are derived for both NOMA and OMA systems. In addition, we also provide tight beta distribution approximations of the meta distributions.
- 3) Next, we derive the distributions of the transmission rates of the CC and CE users along with the CSR under NRT services. In addition, the upper bounds on the distributions of the mean transmission delays of the CC and CE users along with the lower bound on the SEC under RT services are derived.
- 4) As the intermediate results of rate and delay analysis, the exact expressions of the moments and approximate distributions of the areas of the CC and CE regions are derived.
- 5) Finally, we consider two optimization problems for the RA under NRT and RT services, respectively, 1) CSR maximization subject to a minimum transmission rate constraints, and 2) SEC maximization subject to a minimum packet arrival rate constraints.
- 6) Our results demonstrate that, in general, NOMA provides improved rate region and higher CSR as compared to OMA. On the contrary, we show that the NOMA provides improved SEC as compared to OMA only for the higher user density.

II. SYSTEM MODEL

A. Network Modeling

We model the locations of BSs using the homogeneous PPP Φ with density λ . Assuming the strongest mean power based BS association policy, the coverage region of the BS at $\mathbf{x} \in \Phi$

becomes the PV cell V_x which is given by

$$V_x = \{y \in \mathbb{R}^2 : \|y - x\| \leq \|y - x'\|, \forall x' \in \Phi\}.$$

Let V_{xc} and V_{xe} be the CC and CE regions, respectively, of the PV cell V_x corresponding to the BS at $x \in \Phi$, which are defined as follows:

$$V_{xc} = \{y \in V_x : \|y - x\| \leq \min_{x' \in \Phi_x} \tau \|y - x'\|\} \text{ and } V_{xe} = \{y \in V_x : \|y - x\| > \min_{x' \in \Phi_x} \tau \|y - x'\|\}, \quad (1)$$

where $\Phi_x = \Phi \setminus \{x\}$ and $\tau \in (0, 1)$ is the boundary threshold. Fig. 1 (left) depicts the CC and CE regions for $\tau = 0.7$. Now, similar to [38], extending the application of the Type I user point process [39], we define the point processes of the locations of the CC and CE users as

$$\Psi_{cc} = \{U(V_{xc}; N_{xc}) : x \in \Phi\} \text{ and } \Psi_{ce} = \{U(V_{xe}; N_{xe}) : x \in \Phi\}, \quad (2)$$

respectively, where $U(A; N)$ denotes N points chosen independently and uniformly at random from the set A . Here, N_{xc} and N_{xe} are the number of CC users in V_{oc} and CE users in V_{oe} , respectively, which are assumed to follow the zero-truncated Poisson distribution with density ν units per meter². We refer to N_{xc} and N_{xe} as the *CC* and *CE loads* of the BS at x . Since by the Slivnyak's theorem, conditioning on a point is the same as adding a point to the PPP, we consider that the nucleus of the *typical cell* of the point process $\Phi \cup \{o\}$ is located at the origin o . Thus, the typical cell become $V_o = \{y \in \mathbb{R}^2 \mid \|y - x\| > \|y\| \forall x \in \Phi\}$. Using the above construction, the locations the *typical CC user* and the *typical CE user* of Ψ_{cc} and Ψ_{ce} can be modeled using the uniformly distributed points in V_{oc} and V_{oe} , respectively. Thus, Φ becomes the point process of the interfering BSs as seen by the typical CC and CE users.

Let $R_o = \|y\|$ be the *service link distance*, i.e., the distance between the user at $y \in V_o$ and its serving BS at o . Let $R_d = \|x_d - y\|$ be the distance from the user at $y \in V_o$ to its dominant interfering BS at $x_d \in \Phi$ where $x_d = \arg \max_{x \in \Phi} \|x - y\|^{-\alpha}$ and α is the path-loss exponent. Therefore, the definitions given in (1) and (2) implicitly classify the CC and CE users based on their distances (i.e., path-losses) from their serving and dominant interfering BSs such that the CC user at $y \in V_{oc}$ has $R_o \leq \tau R_d$ and the CE user at $y \in V_{oe}$ has $R_o > \tau R_d$. Fig. 1 (Left) illustrates a typical realization of Ψ_{cc} and Ψ_{ce} . From this figure, it is clear that (1) accurately preserves the CC and CE regions wherein the SIR is expected to be higher and lower,

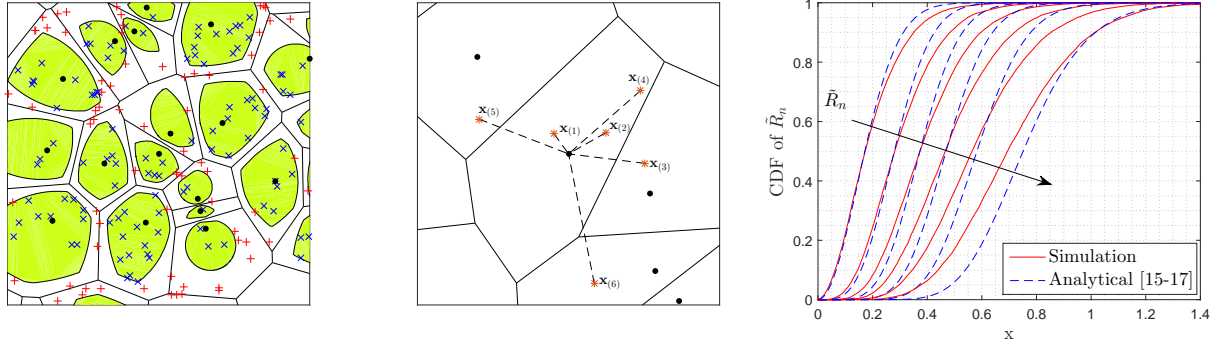


Figure 1. Left: Simulation of Ψ_{cc} and Ψ_{ce} for $\tau = 0.7$, $\lambda = 1$, and $\nu = 20$. Middle: an illustration of the user cluster from [15]–[17] for $N = 6$ (and of the fact that it is not necessarily confined in the PV cell). Right: the distributions of the ordered link distances modeled in [15]–[17] for $N = 6$ and $\lambda = 1$. The dot, cross, plus, and star markers correspond to BSs, CC users, CE users, and user cluster, respectively. The green and white colors in the left figure represent the CC and CE regions.

respectively. As a comparison, Fig. 1 (Middle) illustrates a realization of a user cluster that results from the distance-based ranking scheme of [15]–[17]. As is clearly evident from the figure, the user cluster is not confined to the PV cell, which is an unintended consequence of ignoring correlation in the user locations. This can also be verified by comparing the distributions of the ordered distances used in [15]–[17] with those obtained from the simulations. This comparison is given in Fig. 1 (Right) wherein \tilde{R}_n is the link distance of the n -th closest user from the BS.

It should be noted here that the aforementioned clusters are different from the *geographical* clustering of users and BSs that has been recently modeled using PCPs, e.g., see [40], [41]. While the PCPs are useful in capturing the spatial coupling in the locations of the users and BSs, they do not necessarily partition users in different groups based on their QoS as done in the above scheme. Therefore, the proposed technique to form user clusters is applicable to more general studies that may rely on user partitioning based on QoS, such as soft frequency reuse [22]. With this background, we now discuss the downlink NOMA transmission for a randomly selected pair of the CC and CE users in the typical cell in the following subsection.

B. Downlink NOMA Transmission based on the Proposed User Pairing

Each BS is assumed to transmit signal superimposed of two layers corresponding to the messages for the CC and CE users forming a user cluster. Henceforth, the layers intended for the CC and CE users are referred as the L_c and L_e layers, respectively. The L_c and L_e layers are encoded at power levels of θP and $(1 - \theta)P$, respectively, where P is the transmission power per RB and $\theta \in (0, 1)$. Without loss of generality, we assume $P = 1$ (since we ignore thermal noise).

Usually, NOMA allocates more power to the weaker user so that it receives smaller intra-cell interference power compared to the desired signal power. Thus, the CC user first decodes the L_e layer while treating the power assigned to the L_c layer as interference. After successfully decoding the L_e layer, the CC user cancels its signal using SIC from the received signal and then decodes the L_c layer. The SIRs of the typical CC user for decoding the L_c and L_e layers are

$$\text{SIR}_e = \frac{h_{\mathbf{x}_o} R_o^{-\alpha} (1 - \theta)}{\theta h_{\mathbf{x}_o} R_o^{-\alpha} + I_\Phi} \text{ and } \text{SIR}_c = \frac{h_{\mathbf{x}_o} R_o^{-\alpha} \theta}{I_\Phi}, \quad (3)$$

respectively, where $I_\Phi = \sum_{\mathbf{x} \in \Phi} \theta h_{\mathbf{x}} \|\mathbf{x}\|^{-\alpha} + (1 - \theta) h_{\mathbf{x}} \|\mathbf{x}\|^{-\alpha}$ and $h_{\mathbf{x}} \sim \exp(1)$ are i.i.d. fading channel gains. Besides, the CE user decodes L_e layer while treating the power assigned to the L_c layer as interference. Thus, the effective SIR of the typical CE user is also SIR_e given in (3). Note that we implicitly assumed a full-buffer system in (3), which is a common assumption in the stochastic geometry literature and is quite reasonable for NRT services for which the objective is to maximize the sum rate. We will further argue in Subsection II-D that this simple setting also provides useful bounds on the delay-centric metrics.

C. Meta Distribution for the Downlink NOMA System

The success probabilities for the CC and CE users are defined as the probabilities that the typical CC and CE users are able to decode their intended messages. While this allows to determine the mean success probabilities of the typical CC and CE users, it does not provide any information on the disparity in the link performance of the CC and CE users across the network. For that purpose, the distribution of the conditional success probability (conditioned on the locations of BS w.r.t. to the CC/CE user location) can be used. This distribution of the conditional success probability is referred to as the *meta distribution* [19]. The meta distribution for the CC/CE user can be used to answer questions like what percentage of the CC/CE users can establish their links with the transmission reliability above a predefined threshold for a given SIR threshold. Building on the definition of the meta distribution in [19], we define the meta distributions for the CC and CE users under NOMA as below.

Definition 1. *The meta distribution of the typical CC user's success probability is defined as*

$$\bar{F}_c(\beta_c, \beta_e; x) = \mathbb{P}[p_c(\beta_c, \beta_e \mid \mathbf{y}, \Phi) > x], \quad (4)$$

and the meta distribution of the typical CE user's success probability is defined as

$$\bar{F}_e(\beta_e; x) = \mathbb{P}[p_e(\beta_e | \mathbf{y}, \Phi) > x], \quad (5)$$

where $x \in [0, 1]$, β_c and β_e are the SIR thresholds corresponding to the L_c and L_e layers, respectively. $p_c(\beta_c, \beta_e | \mathbf{y}, \Phi) = \mathbb{P}[\text{SIR}_c \geq \beta_c, \text{SIR}_e \geq \beta_e | \mathbf{y}, \Phi]$ and $p_e(\beta_e | \mathbf{y}, \Phi) = \mathbb{P}[\text{SIR}_e \geq \beta_e | \mathbf{y}, \Phi]$ are the success probabilities of the typical CC and CE users conditioned on their locations at \mathbf{y} and the point process Φ of the interfering BSs, respectively.

D. Traffic Modeling, Scheduling, and Performance Metrics

For the above setting, we will perform a comprehensive load-aware performance analysis of the CC/CE users under NOMA system. For this, we consider *random scheduling* wherein each BS randomly selects a pair of CC and CE users within its PV cell for the NOMA transmission in a given time slot. For the NRT services, our objective is to maximize the sum-rate under the NOMA scheme described above. Since the network is assumed to be static, the load-aware transmission rate of CC/CE user at \mathbf{y} depends on its *scheduling probability* and *successful transmission probability* both conditioned on Φ . As already implied above, each CC/CE user within a given cell is equally likely to be scheduled in each time slot and the conditional successful transmissions are i.i.d. across the time slots. Thus, the transmission rates of the CC and CE users located at $\mathbf{y} \in V_o$, given Φ , respectively become

$$R_c(\mathbf{y}, \Phi) = \frac{p_c(\beta_c, \beta_e | \mathbf{y}, \Phi)}{N_{oc}} \log_2(1 + \beta_c) \text{ and } R_e(\mathbf{y}, \Phi) = \frac{p_e(\beta_c, \beta_e | \mathbf{y}, \Phi)}{N_{oe}} \log_2(1 + \beta_e). \quad (6)$$

The characterization of success probability of the typical CC/CE user under the full-buffer system is also useful in obtaining an upper bound on its delay performance for more general traffic patterns. This can subsequently be used to derive lower bounds on the SEC for the given RT service. Since the exact delay analysis for the cellular networks is known to be challenging because of the coupled queues at different BSs, their performance is often studied by employing meaningful *modifications* to the system [42]; see [43]–[45] for a small subset of relevant works. Most of the times, these modifications end up decoupling the queues by assuming that there are always packets being transmitted on the interfering links, which is consistent with what we assumed from the very beginning. Since this effectively underestimates the success probability, it

provides an upper bound on the packet transmission delay. In the same spirit, this paper presents an upper bound on the distribution of the conditional mean delay of the typical link, which is especially accurate for the higher load scenarios. While one can of course determine the mean delay of the typical link by adopting more sophisticated analyses, such as the mean cell approach [46], the contributions of this paper revolve around a new user ranking scheme and the typical cell approach because of which these other approaches are out of the scope of the current paper. Now, in order to perform the delay analysis in the typical cell, we assume that the typical CC/CE user has a dedicated queue of infinite length at its serving BS whose arrival process follows the Bernoulli distribution with mean of ϱ_c/ϱ_e packets per slot and its the packet size is equal to $TB \log_2(1 + \beta_c)/TB \log(1 + \beta_e)$ bits, where T is the slot duration and B is the channel bandwidth. Thus, for this NOMA setup, the successful packet transmission rates, in packets per slot, of the typical CC and CE at $\mathbf{y} \in V_{oc}$ given Φ are, respectively,

$$\mu_c(\mathbf{y}, \Phi) = \frac{p_c(\beta_c, \beta_e \mid \mathbf{y}, \Phi)}{N_{oc}} \text{ and } \mu_e(\mathbf{y}, \Phi) = \frac{p_e(\beta_e \mid \mathbf{y}, \Phi)}{N_{oe}}. \quad (7)$$

Besides, we also analyze the load-aware performances of the CC and CE users under above discussed services for the OMA system, wherein we consider that each BS schedules one of its associated CC (CE) users that is chosen uniformly at random in a given time slot if $r \leq \eta$ ($r > \eta$) where $r \sim U([0, 1])$. The parameter η allows to control the frequency of scheduling of the CC and CE users in order to meet their QoS requirements. The CC/CE load of the typical cell, and hence the scheduling probability of typical CC/CE user, depend on Φ (see (2)). Thus, from (6)-(7), it is quite evident that the exact load aware analysis requires the joint statistical characterization of the success probability and scheduling probability. However, such joint characterization is challenging as the distribution (even the moments) of the area of the PV cell V_o conditioned on the location of the user at $\mathbf{y} \in V_o$ is difficult to obtain. Hence, similar to [38], [45], we adopt the following reasonable assumption in our analysis.

Assumption 1. *We assume that the CC/CE load (or, the scheduling probability) and the successful transmission probability observed by the typical CC/CE user are independent.*

The numerical results presented in Section VI will demonstrate the accuracy of this assumption for the analysis of the metrics discussed above. Now, we analyze the meta distributions for the

CC and CE users in the following section.

III. META DISTRIBUTION ANALYSIS FOR THE CC AND CE USERS

The main goal of this section is to present the downlink meta distribution analysis for NOMA system. As stated already in Section I-B, we characterize the performance of the *typical cell* and our approach departs significantly from the standard stochastic geometry approach of analyzing the performance of a typical user. The key intermediate step in the meta distribution analysis of the typical user in the typical cell is the joint characterization of the service link distance $R_o = \|\mathbf{y}\|$, where $\mathbf{y} \sim U(V_o)$, and the point process Φ of the interfering BSs. Hence, to enable the analysis of the meta distributions of the CC and CE users in the typical cell, we require the joint characterizations of R_o and Φ under the conditions of $R_o \leq R_d\tau$ and $R_o > R_d\tau$. For this, we first determine the marginal and joint probability density functions (pdfs) of R_o and R_d for the CC and CE users. However, given the complexity of the analysis of r.v. R_o [47], it is reasonable to assume that the exact joint characterization of R_o and R_d is equally, if not more, challenging. In fact, the marginal distribution of R_o is generally approximated using the contact distribution with a correction factor (c.f.) in order to maintain tractability [39], [48]. Thus, similar to this, we approximate the joint pdf of R_o and R_d using the joint pdf of the distances to the two nearest points in PPP as

$$f_{R_o, R_d}(r_o, r_d) = (2\pi\rho\lambda)^2 r_o r_d \exp(-\pi\rho\lambda r_d^2), \quad (8)$$

for $r_d \geq r_o \geq 0$ where $\rho = \frac{9}{7}$ is the c.f.

Lemma 1. *The probabilities that a user uniformly distributed in the typical cell is the CC user and the CE user are equal to τ^2 and $1 - \tau^2$, respectively. The cumulative density function (CDF) of R_o and the CDF of R_d conditioned on R_o for the CC user are given by*

$$F_{R_o}^c(r_o) = 1 - \exp(-\pi\rho\lambda r_o^2/\tau^2) \quad (9)$$

$$\text{and } F_{R_d|R_o}^c(r_d | r_o) = 1 - \exp(-\pi\rho\lambda(r_d^2 - r_o^2/\tau^2)) \quad (10)$$

for $r_o > 0$ and $r_d > \frac{r_o}{\tau}$, respectively. The joint pdf of R_o and R_d for the CC user is given by

$$f_{R_o, R_d}^c(r_o, r_d) = \frac{(2\pi\rho\lambda)^2}{\tau^2} r_o r_d \exp(-\pi\rho\lambda r_d^2) \quad \text{for } r_d > \frac{r_o}{\tau} \text{ and } r_o > 0. \quad (11)$$

The CDF of R_o and the CDF of R_d conditioned on R_o for the CE user are respectively given by

$$F_{R_o}^e(r_o) = 1 - \frac{\exp(-\pi\rho\lambda r_o^2)}{1 - \tau^2} [1 - \tau^2 \exp(-\pi\rho\lambda r_o^2(\tau^{-2} - 1))] \text{ for } r_o > 0, \quad (12)$$

$$\text{and } F_{R_d|R_o}^e(r_d | r_o) = \begin{cases} \frac{1 - \exp(-\pi\rho\lambda(r_d^2 - r_o^2))}{1 - \exp(-\pi\rho\lambda r_o^2(\tau^{-2} - 1))} & \text{for } \frac{r_o}{\tau} > r_d \geq r_o, \\ 1 & \text{for } r_d \geq \frac{r_o}{\tau}. \end{cases} \quad (13)$$

The joint pdf of R_o and R_d for the CE user is given by

$$f_{R_o, R_d}^e(r_o, r_d) = \frac{(2\pi\rho\lambda)^2}{1 - \tau^2} r_o r_d \exp(-\pi\rho\lambda r_d^2) \quad \text{for } \frac{r_o}{\tau} \geq r_d > r_o \text{ and } r_o > 0. \quad (14)$$

Proof. Please refer to Appendix A. \square

A. Meta Distribution for CC and CE users

As the CC users need to jointly decode both the L_c and L_e layers, the successful transmission event for the CC user is given by

$$\mathcal{E}_c = \{\text{SIR}_c > \beta_c\} \cap \{\text{SIR}_e > \beta_e\} = \{h_{\mathbf{x}_o} > R_o^\alpha I_\Phi \chi_c\}, \quad (15)$$

where $\chi_c = \max\left\{\frac{\beta_c}{\theta}, \frac{\beta_e}{1-\theta(1+\beta_e)}\right\}$. On the other hand, the CE user decodes its message while treating the signal intended for the CC user as the interference power. Thus, the successful transmission event for the CE user is given by

$$\mathcal{E}_e = \{\text{SIR}_e > \beta_e\} = \{h_{\mathbf{x}_o} > R_o^\alpha I_\Phi \chi_e\}, \quad (16)$$

where $\chi_e = \frac{\beta_e}{1-\theta(1+\beta_e)}$. It is easy to interpret that the interference due to the non-orthogonal transmission reduces the effective transmission power for decoding the L_e layer which decreases the chance of successful transmission. Since it is difficult to directly derive the meta distribution [19], we first derive the moments of the meta distribution in the following theorem and then use them to approximate the meta distribution.

Theorem 1. The b -th moments of the meta distributions of conditional success probability for the typical CC and CE users under NOMA respectively are

$$M_b^c(\chi_c) = \frac{\rho^2}{\tau^2} \int_0^{\tau^2} \frac{(\rho + v \mathcal{Z}_b(\chi_c, v))^{-2}}{(1 + \chi_c v^{\frac{1}{\theta}})^b} dv \text{ and } M_b^e(\chi_e) = \frac{\rho^2}{1 - \tau^2} \int_{\tau^2}^1 \frac{(\rho + v \mathcal{Z}_b(\chi_e, v))^{-2}}{(1 + \chi_e v^{\frac{1}{\theta}})^b} dv, \quad (17)$$

where $\delta = \frac{2}{\alpha}$, and $\mathcal{Z}_b(\chi, a) = \chi^\delta \int_{\chi^{-\delta}a^{-1}}^{\infty} \left[1 - (1 + t^{-\frac{1}{\delta}})^{-b}\right] dt$.

Proof. Please refer to Appendix B. \square

In OMA, each BS serves its associated users using orthogonal RBs which means that there is no intra-cell interference. Thus, OMA provides the better success probabilities for the CC and CE users compared to NOMA. However, the orthogonal RB allocation reduces the transmission instances for the CC and CE users which degrades their transmission rates. The successful transmission events for the CC and CE user under OMA respectively are

$$\tilde{\mathcal{E}}_c = \{h_{\mathbf{x}_o} > R_o^\alpha \beta_c I_\Phi\} \text{ and } \tilde{\mathcal{E}}_e = \{h_{\mathbf{x}_o} > R_o^\alpha \beta_e I_\Phi\}. \quad (18)$$

The following corollary presents the b -th moments of the meta distributions for OMA case.

Corollary 1. *The b -th moments of the meta distributions of conditional success probability for the typical CC and CE users under OMA respectively are*

$$\tilde{M}_b^c(\beta_c) = \frac{\rho^2}{\tau^2} \int_0^{\tau^2} \frac{(\rho + v\mathcal{Z}_b(\beta_c, v))^{-2}}{(1 + \beta_c v^{\frac{1}{\delta}})^b} dv \text{ and } \tilde{M}_b^e(\beta_e) = \frac{\rho^2}{1 - \tau^2} \int_{\tau^2}^1 \frac{(\rho + v\mathcal{Z}_b(\beta_e, v))^{-2}}{(1 + \chi_e v^{\frac{1}{\delta}})^b} dv, \quad (19)$$

where $\delta = \frac{2}{\alpha}$, and $\mathcal{Z}_b(\beta, a) = \beta^\delta \int_{\beta^{-\delta}a^{-1}}^{\infty} \left[1 - (1 + t^{-\frac{1}{\delta}})^{-b}\right] dt$.

Proof. Using the definitions in (18) and following the steps in Appendix B, we obtain (19). \square

Fig. 2 verifies that the means and variances of the meta distributions of the CC and CE users under NOMA (Left) and OMA (Middle) derived in Theorem 1 and Corollary 1, respectively, closely match with the simulation results. The moments for the CE user monotonically decrease with θ as the interference from the L_c layer increases with θ . However, the performance trend of the moments for the CC user w.r.t. θ is different. This is because θ has opposite effects on the ability of decoding the L_c and L_e layers at the CC user. While increasing θ makes it difficult to decode L_e layer, it also makes it easier to decode L_c layer. As a result, the impact of L_c layer decoding is dominant for $\theta \leq \hat{\theta}$ ($= 0.5$ for $(\beta_c, \beta_e) = (0, -3)$ (in dB)) and the impact of L_e layer decoding is dominant for $\theta > \hat{\theta}$ where $\hat{\theta}$ will be defined in Section V.

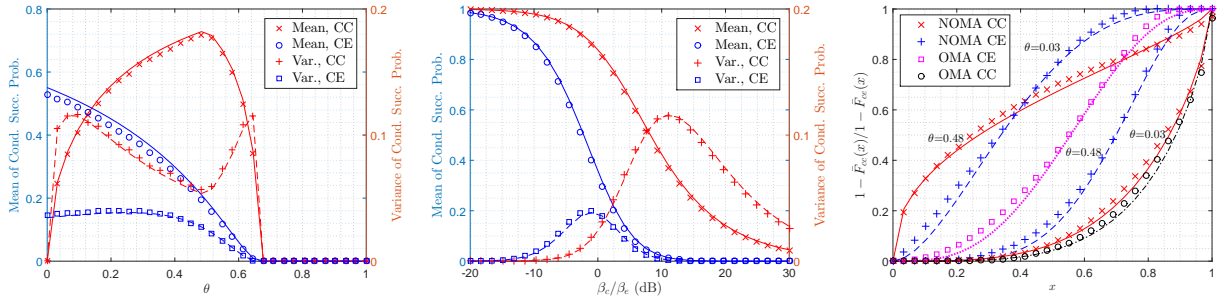


Figure 2. Moments for the CC and CE users under NOMA (Left) and OMA (Middle), and the beta approximations (Right) for $\tau = 0.7$, $\alpha = 4$, $\lambda = 1$, and $(\beta_c, \beta_e) = (0, -3)$ dB. The solid and dashed curves correspond to the analytical results and the markers correspond to the simulation results.

B. Meta Distribution and its Approximation

Using M_b^c and M_b^e derived in Theorem 1 and the Gil-Pelaez's inversion theorem [49], the exact meta distributions for the typical CC and CE users under NOMA can be obtained. However, the evaluation of meta distributions using the Gil-Pelaez inversion is computationally complex. Thus, similar to [19], by matching the moments, we approximate the meta distributions of the CC and CE users with the beta distributions as

$$\bar{F}_c(\chi_c; x) \approx 1 - I(x; \kappa_{1c}, \kappa_{2c}) \text{ and } \bar{F}_e(\chi_e; x) \approx 1 - I(x; \kappa_{1e}, \kappa_{2e}), \quad (20)$$

respectively, where $I(x; a, b)$ is the regularized incomplete beta function and $\kappa_{1s} = \frac{M_1^s \kappa_{2s}^{ss}}{1 - M_1^s}$ and $\kappa_{2s} = \frac{(M_1^s - M_2^s)(1 - M_1^s)}{M_2^s - (M_1^s)^2}$ such that $s = \{c, e\}$. Similarly, the beta approximations for the meta distributions under OMA can be obtained using the moments given in Corollary 1. We denote the parameters of the beta approximations of the CC (CE) users under OMA by $\tilde{\kappa}_{1c}$ and $\tilde{\kappa}_{1e}$ ($\tilde{\kappa}_{1e}$ and $\tilde{\kappa}_{1e}$). Fig. 2 (Right) shows that the beta distribution closely approximate the meta distributions of the CC and CE users for both NOMA and OMA. The proposed beta approximations can be used for the system-level analysis without having to perform the computationally complex Gil-Pelaez inversion. We also observe that the percentage of the CE users meeting the link reliability threshold (i.e., the conditional success probability threshold) drops with increasing θ whereas the percentage of CC users meeting the link reliability threshold increases with θ , as expected.

IV. THROUGHPUT AND DELAY ANALYSIS FOR THE CC AND CE USERS

In this section, we characterize the conditional transmission rate (given in (6)) and the conditional mean delay (given in (7)) of the CC/CE users under NRT and RT services, respectively, for both NOMA and OMA systems. For this, we first derive the distributions of the CC and CE loads in the following subsection.

A. Distributions of the CC and CE Loads

The CC and CE loads of the typical cell V_o , i.e., N_{oc} and N_{oe} , depend on the areas of CC and CE regions, i.e., $|V_{oc}|$ and $|V_{oe}|$. We first drive the exact first two moments of these areas in the following lemma as it is difficult to directly derive the area distributions of such random sets.

Lemma 2. *For a given τ , the mean areas of the CC and CE regions are, respectively,*

$$\mathbb{E}[|V_{oc}|] = \tau^2 \lambda^{-1} \text{ and } \mathbb{E}[|V_{oe}|] = (1 - \tau^2) \lambda^{-1}, \quad (21)$$

and second moments of the areas of the CC and CE regions are, respectively,

$$\mathbb{E}[|V_{oc}|^2] = 4\pi \int_0^\pi \int_0^\infty \int_0^\infty \exp(-\lambda U_3) r_1 dr_1 r_2 dr_2 du \text{ and } \mathbb{E}[|V_{oe}|^2] = 4\pi \int_0^\pi \int_0^\infty \mathcal{F}(r_2, u) r_2 dr_2 du, \quad (22)$$

$$\begin{aligned} \text{where } \mathcal{F}(r_2, u) = & \int_{\mathbb{D}(r_2, u)} (\exp(-\lambda U_1) \mathbb{1}_{r_1 \leq r_2} + \exp(-\lambda U_2) \mathbb{1}_{r_2 < r_1}) r_1 dr_1 + \int_{\mathbb{R} \setminus \mathbb{D}(r_2, u)} ([\exp(-\lambda U_o) \\ & - \exp(-\lambda(U_1 + U_2 - U_3))] + [\exp(-\lambda(U_2 - U_3) - 1) [\exp(-\lambda U_1) - \exp(-\lambda U_3)])] r_1 dr_1, \end{aligned}$$

$$\begin{aligned} \mathbb{D}(r_2, u) &= \{r_1 \in \mathbb{R} : d \leq \tau^{-1} |r_1 - r_2|\}, \quad d = (r_1^2 + r_2^2 - 2r_1 r_2 \cos(u))^{\frac{1}{2}}, \\ U_o &= U(r_1, r_2, u_o), \quad U_3 = U(r_1 \tau^{-1}, r_2 \tau^{-1}, u_3), \quad U_1 = U(r_1 \tau^{-1}, r_2, u_1) \text{ if } r_1 \tau^{-1} < d + r_2 \text{ otherwise } U_1 = \pi r_1^2 \tau^{-2}, \\ U_2 &= U(r_1, r_2 \tau^{-1}, u_2) \text{ if } r_2 \tau^{-1} < d + r_1 \text{ otherwise } U_2 = \pi r_2^2 \tau^{-2}, \\ u_o &= u, \quad u_1 = \arccos\left((\tau^{-1} - \tau) \frac{r_1}{2r_2} + \tau \cos(u)\right), \quad u_2 = \arccos\left((\tau^{-1} - \tau) \frac{r_2}{2r_1} + \tau \cos(u)\right), \\ u_3 &= \arccos\left((1 - \tau^2) \frac{r_1^2 + r_2^2}{2r_1 r_2} + \tau^2 \cos(u)\right), \\ U(r_1, r_2, u) &= r_1^2 \left(\pi - w(r_1, r_2, u) + \frac{\sin(2w(r_1, r_2, u))}{2}\right) + r_2^2 \left(\pi - w(r_2, r_1, u) + \frac{\sin(2w(r_2, r_1, u))}{2}\right), \\ \text{and } w(r_1, r_2, u) &= \arccos(d^{-1}(r_1 - r_2 \cos(u))). \end{aligned}$$

Proof. Please refer to Appendix C. □

Now, using the moments derived in Lemma 2, we approximate the distributions of the CC and CE areas. Since the area of the PV cell is empirically shown to follow gamma distribution [50],

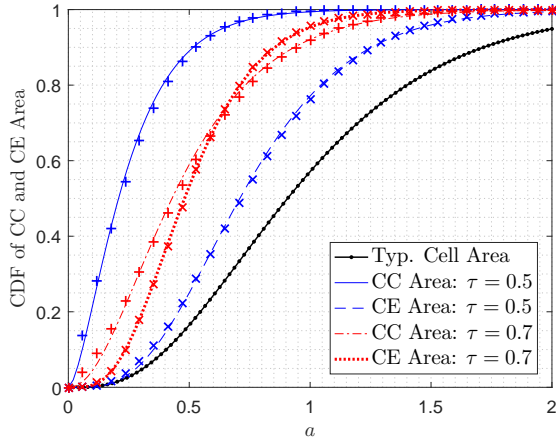


Figure 3. Gamma approximation of the area distributions of the CC and CE regions. The solid and dashed curves correspond to the gamma approximations and the markers correspond to the simulation results.

it is the natural first choice for the approximations of the distributions of the CC and CE areas as the sum of two independent gamma distributed random variables is also gamma distributed and the correlation between the CC and CE areas is not too high. Thus, pdfs of the CC and CE areas are, respectively, approximated as

$$f_{|V_{oc}|}(a) = \frac{\gamma_{1c}^{\gamma_{2c}}}{\Gamma(\gamma_{2c})} a^{\gamma_{2c}-1} \exp(-\gamma_{1c}a) \text{ and } f_{|V_{oe}|}(a) = \frac{\gamma_{1e}^{\gamma_{2e}}}{\Gamma(\gamma_{2e})} a^{\gamma_{2e}-1} \exp(-\gamma_{1e}a), \quad (23)$$

where $\gamma_{2c} = \gamma_{1c} \mathbb{E}[|V_{oc}|]$, $\gamma_{1c} = \frac{\mathbb{E}[|V_{oc}|]}{\mathbb{E}[|V_{oc}|^2] - \mathbb{E}[|V_{oc}|]^2}$, $\gamma_{2e} = \gamma_{1e} \mathbb{E}[|V_{oe}|]$, and $\gamma_{1e} = \frac{\mathbb{E}[|V_{oe}|]}{\mathbb{E}[|V_{oe}|^2] - \mathbb{E}[|V_{oe}|]^2}$. Fig. 3 provides the visual verification of the gamma approximations given in (23) for $\tau \in \{0.5, 0.7\}$. Using (23), the distributions of the CC and CE loads are obtained in the following lemma.

Lemma 3. *The probability mass function (pmf) of the number of CC users, i.e., N_{oc} , is*

$$\mathbb{P}[N_{oc} = n] = \frac{\nu^n \gamma_{1c}^{\gamma_{2c}}}{n! \Gamma(\gamma_{2c})} \int_0^\infty a^{n+\gamma_{2c}-1} \frac{\exp(-(\nu + \gamma_{1c})a)}{1 - \exp(-\nu a)} da \quad (24)$$

where γ_{1c} and γ_{2c} are given in (23). The pmf of the number of CE, i.e., N_{oe} , is

$$\mathbb{P}[N_{oe} = n] = \frac{\nu^n \gamma_{1e}^{\gamma_{2e}}}{n! \Gamma(\gamma_{2e})} \int_0^\infty a^{n+\gamma_{2e}-1} \frac{\exp(-(\nu + \gamma_{1e})a)}{1 - \exp(-\nu a)} da \quad (25)$$

where γ_{1e} and γ_{2e} are given in (23).

Proof. For given $|V_{oc}|$, N_{oc} follows zero-truncated Poisson with mean $\nu|V_{oc}|$. Thus, we have

$$\mathbb{P}[N_{oc} = n] = \mathbb{E}_{|V_{oc}|} [\mathbb{P}[N_{oc} = n \mid |V_{oc}|]] \text{ for } n > 0.$$

Thus, the pmf of N_{oc} given in (24) follows using the pdf of $|V_{oc}|$ given in (23). Similarly, the pmf of N_{oe} given in (25) follows using the pdf of $|V_{oe}|$ given in (23). \square

B. Transmission Rates of the CC and CE Users

In this subsection, we derive the distributions of the conditional transmission rates of the CC and CE users under random scheduling which are, respectively, defined as

$$\mathcal{R}_c(\mathbf{r}_c; \chi_c) = \mathbb{P}[R_c(\mathbf{y}, \Phi) \leq \mathbf{r}_c] \text{ and } \mathcal{R}_e(\mathbf{r}_e; \chi_e) = \mathbb{P}[R_e(\mathbf{y}, \Phi) \leq \mathbf{r}_e], \quad (26)$$

where $R_c(\mathbf{y}, \Phi)$ and $R_e(\mathbf{y}, \Phi)$ are given in (6). Therefore, using Assumption 1 along with the meta distributions (given in Section III-B) and the pmf of the cell load (given in Section IV-A), we derive the means and distributions of the conditional transmission rates of the CC and CE users in the following theorem.

Theorem 2. *The mean transmission rates of the typical CC and CE users under NOMA are*

$$\bar{R}_c(\chi_c) = \xi_c \log_2 (1 + \beta_c) M_1^c(\chi_c, 1) \text{ and } \bar{R}_e(\chi_e) = \xi_e \log_2 (1 + \beta_e) M_1^e(\chi_e, 1), \quad (27)$$

respectively, where $M_1^c(\chi_c, 1)$ and $M_1^e(\chi_e, 1)$ are given in (17), $s \in \{c, e\}$, $\xi_s = \sum_{n=1}^{\infty} \frac{1}{n} \mathbb{P}[N_{os} = n]$, and $\mathbb{P}[N_{os} = n]$ is given in Lemma 3. The CDF of the conditional transmission rates of the typical CC and CE users under NOMA are, respectively,

$$\mathcal{R}_c(\mathbf{r}_c; \chi_c) = \mathbb{E}_{N_{oc}} [I(\min(\mathbf{r}_c N_{oc} \log_2(1 + \beta_c)^{-1}, 1); \kappa_{1c}, \kappa_{2c})], \quad (28)$$

$$\text{and } \mathcal{R}_e(\mathbf{r}_e; \chi_e) = \mathbb{E}_{N_{oe}} [I(\min(\mathbf{r}_e N_{oe} \log_2(1 + \beta_e)^{-1}, 1); \kappa_{1e}, \kappa_{2e})], \quad (29)$$

where $s \in \{c, e\}$, κ_{1s} and κ_{2s} are given in (20), and $\mathbb{P}[N_{os} = n]$ is given in Lemma 3.

Proof. Please refer to Appendix D. \square

For OMA, we consider that each BS serves its associated CC and CE users respectively for η and $1 - \eta$ fractions of time in order to control the cell throughput and maintain certain level of QoS. Note that for $\eta = \frac{|V_{oc}|}{|V_o|}$ and higher $\frac{\nu}{\lambda}$, the above OMA scheduling scheme will be

almost equivalent to the random scheduling wherein the typical BS randomly schedules one of its associated users in a given time slot.

Corollary 2. *The mean transmission rates of the typical CC and CE users under OMA are*

$$\tilde{R}_c(\beta_c) = \eta \xi_c \log_2 (1 + \beta_c) \tilde{M}_1^c(\beta_c, 1) \text{ and } \tilde{R}_e(\beta_e) = (1 - \eta) \xi_e \log_2 (1 + \beta_e) \tilde{M}_1^e(\beta_e, 1), \quad (30)$$

respectively, where $\tilde{M}_1^c(\chi_c, 1)$ and $\tilde{M}_1^e(\chi_e, 1)$ are given in (19) and, $s \in \{c, e\}$, $\xi_s = \sum_{n=1}^{\infty} \frac{1}{n} \mathbb{P}[N_{os} = n]$, and $\mathbb{P}[N_{os} = n]$ is given in Lemma 3. The CDF of the conditional transmission rates of the typical CC and CE users under OMA respectively are

$$\tilde{\mathcal{R}}_c(\mathbf{r}_c; \beta_c) = \mathbb{E}_{N_{oc}} \left[I \left(\min \left(\mathbf{r}_c \eta^{-1} N_{oc} \log_2 (1 + \hat{\beta}_c)^{-1}, 1 \right); \tilde{\kappa}_{1c}, \tilde{\kappa}_{2c} \right) \right], \quad (31)$$

$$\text{and } \tilde{\mathcal{R}}_e(\mathbf{r}_e; \beta_e) = \mathbb{E}_{N_{oe}} \left[I \left(\min \left(\mathbf{r}_e (1 - \eta)^{-1} N_{oe} \log_2 (1 + \beta_e)^{-1}, 1 \right); \tilde{\kappa}_{1e}, \tilde{\kappa}_{2e} \right) \right], \quad (32)$$

where $s \in \{c, e\}$, $\tilde{\kappa}_{1s}$ and $\tilde{\kappa}_{2s}$ are given in Section III-B, and $\mathbb{P}[N_{os} = n]$ is given in Lemma 3.

C. Delay Analysis of the CC and CE Users

This subsection analyzes the delay performance of the typical CC/CE user for the given RT service under the NOMA setup described in Section II. As discussed in Section II, we assumed saturated queues at the interfering BSs because of which the meta distributions derived in Section III-A can be directly used to analyze the upper bound of the delay performance of the typical CC and CE user. That said, the conditional packet transmission rate of the typical CC/CE user is the product of its scheduling probability and success probability as stated in (7) for given \mathbf{y} and Φ . Since, given \mathbf{y} and Φ , the successful transmissions are independent across the different time slots and the users are scheduled randomly with equal probability, the service times of packets of the typical CC/CE user at \mathbf{y} given Φ are i.i.d. and follow geometric distribution with parameter $\mu_c(\mathbf{y}, \Phi)/\mu_e(\mathbf{y}, \Phi)$. Besides, the packet arrives in each time slot as per the Bernoulli process with mean ϱ_c/ϱ_e . Thus, the queue of the typical CC/CE user can be modeled as the Geo/Geo/1 queue. Given \mathbf{y} and Φ , the mean delays of the typical CC and CE users are [51]

$$D_c(\mathbf{y}, \Phi) = \frac{1 - \varrho_c}{\mu_c(\mathbf{y}, \Phi) - \varrho_c} \mathbb{1}_{\mu_c(\mathbf{y}, \Phi) > \varrho_c} \text{ and } D_e(\mathbf{y}, \Phi) = \frac{1 - \varrho_e}{\mu_e(\mathbf{y}, \Phi) - \varrho_e} \mathbb{1}_{\mu_e(\mathbf{y}, \Phi) > \varrho_e}, \quad (33)$$

respectively. Let t_c and t_e are mean delay thresholds of the CC and CE users, respectively.

Theorem 3. *The complementary CDF (CCDF) of the conditional mean delays of the typical CC and CE users under NOMA with random scheduling are upper bounded respectively by*

$$\mathcal{D}_c(t_c; \chi_c) = \mathbb{E}_{N_{oc}} \left[I \left(\min \left(N_{oc} \left(\frac{1 - \varrho_c}{t_c} + \varrho_c \right), 1 \right); \kappa_{1c}, \kappa_{2c} \right) \right] \quad (34)$$

$$\text{and } \mathcal{D}_e(t_e; \chi_e) = \mathbb{E}_{N_{oe}} \left[I \left(\min \left(N_{oe} \left(\frac{1 - \varrho_e}{t_e} + \varrho_e \right), 1 \right); \kappa_{1e}, \kappa_{2e} \right) \right], \quad (35)$$

where $s \in \{c, e\}$ κ_{1s} and κ_{2s} are given in (20), and $\mathbb{P}[N_{os} = n]$ is given by Lemma 3.

Proof. Using Assumption 1 along with (7) and (33), the CDF of $D_c(\mathbf{y}, \Phi)$ becomes

$$\begin{aligned} \mathbb{P}[D_c(\mathbf{y}, \Phi) < t_c] &= \mathbb{P} \left[\mu_c(\mathbf{y}, \Phi) > \frac{1 - \varrho_c}{t_c} + \varrho_c, \mu_c(\mathbf{y}, \Phi) > \varrho_c \right] \\ &= \mathbb{E}_{N_{oc}} \left[\mathbb{P} \left(p_c(\beta_c, \beta_e | \mathbf{y}, \Phi) > N_{oc} \left(\frac{1 - \varrho_c}{t_c} + \varrho_c \right) | N_{oc} \right) \right] \end{aligned}$$

Now, using the beta approximation of the meta distribution for the system model discussed in Section II-D, we obtain the upper bound of the CCDF of $D_c(\mathbf{y}, \Phi)$ as $\mathcal{D}_c(t_c; \chi_c)$ given in (34). Similarly, we obtain the upper bound of the CCDF of $D_e(\mathbf{y}, \Phi)$ as in (35). \square

For OMA, the mean delay of the typical CC and CE users at \mathbf{y} conditioned on Φ becomes

$$\tilde{\mu}_c(\beta_c | \mathbf{y}, \Phi) = \frac{\eta \mathbb{E} [\mathbb{1}_{\tilde{\mathcal{E}}_c}(\text{SIR}_{cc}) | \mathbf{y}, \Phi]}{N_{oc}} \text{ and } \tilde{\mu}_e(\chi_e | \mathbf{y}, \Phi) = \frac{(1 - \eta) \mathbb{E} [\mathbb{1}_{\tilde{\mathcal{E}}_e}(\text{SIR}_{ce}) | \mathbf{y}, \Phi]}{N_{oe}},$$

The following corollary presents the upper bounds of the outages of conditional mean delays for the OMA case.

Corollary 3. *The CCDF of the mean delays of the typical CC and CE users under OMA with random scheduling are upper bounded respectively by*

$$\tilde{\mathcal{D}}_c(t_c; \chi_c) = \mathbb{E}_{N_{oc}} \left[I \left(\min \left(\eta^{-1} N_{oc} \left(\frac{1 - \varrho_c}{t_c} + \varrho_c \right), 1 \right); \tilde{\kappa}_{1c}, \tilde{\kappa}_{2c} \right) \right] \quad (36)$$

$$\text{and } \tilde{\mathcal{D}}_e(t_e; \chi_e) = \mathbb{E}_{N_{oe}} \left[I \left(\min \left((1 - \eta)^{-1} N_{oe} \left(\frac{1 - \varrho_e}{t_e} + \varrho_e \right), 1 \right); \tilde{\kappa}_{1e}, \tilde{\kappa}_{2e} \right) \right], \quad (37)$$

where $s \in \{c, e\}$, $\tilde{\kappa}_{1s}$ and $\tilde{\kappa}_{2s}$ are given in Section III-B, and $\mathbb{P}[N_{os} = n]$ is given in Lemma 3.

V. OPTIMAL RESOURCE ALLOCATION

In this section, we focus on the RA for maximizing the network performance under both NRT and RT services while meeting the QoS constraints of the CC and CE users. For the NOMA and OMA systems, CSRs can be, respectively, given by

$$\text{CSR}_{\text{NOMA}} = B \log_2(1 + \beta_c) M_1^c(\chi_c, 1) + B \log_2(1 + \beta_e) M_1^e(\chi_e, 1), \quad (38)$$

$$\text{and } \text{CSR}_{\text{OMA}} = \eta B \log_2(1 + \beta_c) \tilde{M}_1^c(\chi_c, 1) + (1 - \eta) B \log_2(1 + \beta_e) \tilde{M}_1^e(\chi_e, 1). \quad (39)$$

Using the upper bounds of the delay distributions given in Section IV-C, the lower bounds of effective capacities of the RT services of the CC and CE users under NOMA and OMA become

$$\text{EC}_{\text{NOMA}}^s = \{\varrho_s \in \mathbb{R}_+ : \mathcal{D}_s(\mathbf{t}_s, \chi_s) = 0_s\} \text{ and } \text{EC}_{\text{OMA}}^s = \{\varrho_s \in \mathbb{R}_+ : \tilde{\mathcal{D}}_s(\mathbf{t}_s, \chi_s) = 0_s\}, \quad (40)$$

respectively, where $s = \{c, e\}$, and the 0_c and 0_e are the delay QoS outage thresholds for the CC and CE users. Now, in the following, we formulate two RA problems with objectives to maximize CSR under NRT services and the lower bound of SEC under RT services such that the QoSs of the CC and CE users under these services are ensured.

1) \mathcal{P}_1 - CSR maximization subject to the minimum mean transmission rates of CC and CE users

$$\begin{array}{ll} \max_{0 < \theta < 1} \text{CSR}_{\text{NOMA}} & \max_{0 < \eta < 1} \text{CSR}_{\text{OMA}} \\ \text{NOMA: s.t. } \bar{R}_c(\chi_c) \geq R_c & \text{OMA: s.t. } \tilde{R}_c(\chi_c) \geq R_c \\ \bar{R}_e(\chi_e) \geq R_e, & \tilde{R}_e(\chi_e) \geq R_e, \end{array}$$

2) \mathcal{P}_2 - SEC maximization

$$\begin{array}{ll} \max_{0 < \theta < 1} \text{EC}_{\text{NOMA}}^c + \text{EC}_{\text{NOMA}}^e & \max_{0 < \eta < 1} \text{EC}_{\text{OMA}}^c + \text{EC}_{\text{OMA}}^e \\ \text{NOMA: s.t. } \text{EC}_{\text{NOMA}}^c \geq \bar{\varrho}_c & \text{OMA: s.t. } \text{EC}_{\text{OMA}}^c \geq \bar{\varrho}_c \\ \text{EC}_{\text{NOMA}}^e \geq \bar{\varrho}_e, & \text{EC}_{\text{OMA}}^e \geq \bar{\varrho}_e. \end{array}$$

While rate QoS constraints are explicitly considered in first problem \mathcal{P}_1 , the delay QoS constraints are implicit in the formulation of the second problem \mathcal{P}_2 . In particular, the effective capacity constraints in \mathcal{P}_2 are considered to ensure the minimum packet arrival rate for the CE users as the SEC maximization might result in the power/time allocation that maximizes only $\text{EC}_{\text{NOMA}}^c / \text{EC}_{\text{OMA}}^c$.

As the above optimization problems do not fall in the standard convex-optimization framework, we provide an efficient method based on the insights obtained from the NOMA analysis to obtain

the near optimal CSR. In order to maximize the CSR, it is natural to allocate the remaining power to the CC user after achieving the minimum transmission rate of the CE user. Thus, we consider to maximize the mean transmission rate of the CC user under the constraints of the minimum transmission rates of the CC and CE users. One can easily see that $\theta \leq \theta_{NC} = (1 + \beta_e)^{-1}$ is the necessary condition for $SIR_e \geq \beta_e$. From (15), we note that the success probability of the CC user increases with the decrease of χ_c and vice-versa. The success probability (thus, the mean transmission rate) of the CC user is an increasing and decreasing function of θ for $0 < \theta \leq \hat{\theta}$ and $\hat{\theta} < \theta \leq \theta_{NC}$ where

$$\hat{\theta} = \underset{0 < \theta \leq \theta_{NC}}{\operatorname{argmin}} \chi_c = \left\{ \theta : \frac{\beta_c}{\theta} = \frac{\beta_e}{1 - \theta(1 + \beta_e)} \right\}. \quad (41)$$

From the above, we know that there are two solutions (if any exists), denoted by θ_{lc} and θ_{uc} , to $\bar{R}_c(\chi_c) = R_c$ such that $\theta_{lc} \leq \hat{\theta}$ and $\theta_{uc} \geq \hat{\theta}$. Further, we also know that the mean transmission rate of the CE user is a monotonically decreasing function of θ . Let θ_e be the solution of $\bar{R}_e(\chi_e) = R_e$. Therefore, from the above discussion, the optimal allocation becomes $\theta^* = \min\{\theta_e, \hat{\theta}\}$ if θ_{lc} and θ_e exist such that $\theta_e \geq \theta_{lc}$. On the other hand, it is straightforward to choose the optimal solution $\eta^* = \eta_e$ for OMA if $\eta_c \leq \eta_e$ where η_c and η_e are the solutions of $\bar{R}_c(\chi_c) = R_c$ and $\bar{R}_e(\chi_e) = R_e$, respectively. This follows from the fact that CSE_{OMA} and mean transmission rate of the CC user are monotonically increasing functions of η and the mean transmission rate of the CE user is a monotonically decreasing function of η . Note that there is no feasible solution if $\eta_c > \eta_e$. Further, the optimal RA under the problem \mathcal{P}_2 can be obtained using similar arguments.

VI. NUMERICAL RESULTS AND DISCUSSION

In this section, we first verify the accuracy of analytical results by comparing them with the simulation results obtained through Monte Carlo simulations of the setup described in Section II. Next, we discuss the performance trends of the achievable CSR, and the transmission rates and mean delays of the CC and CE users for various settings. Further, we also compare the performances of these metrics for the NOMA and OMA systems. For this, we consider $\lambda = 1$, $\nu = 5$, $\alpha = 4$, $\tau = 0.7$, $(\beta_c, \beta_e) = (3, -3)$ in dB, $B = 1$ Hz, $(r_c, r_e) = (0.1, 0.05)$, $(\varrho_c, \varrho_e) = (0.05, 0.05)$, and $(t_c, t_e) = (20, 30)$, unless mentioned otherwise.

Fig. 4 depicts that the mean transmission rates of the CC and CE users closely match with the simulation results for both the NOMA and OMA systems. The curves correspond to the

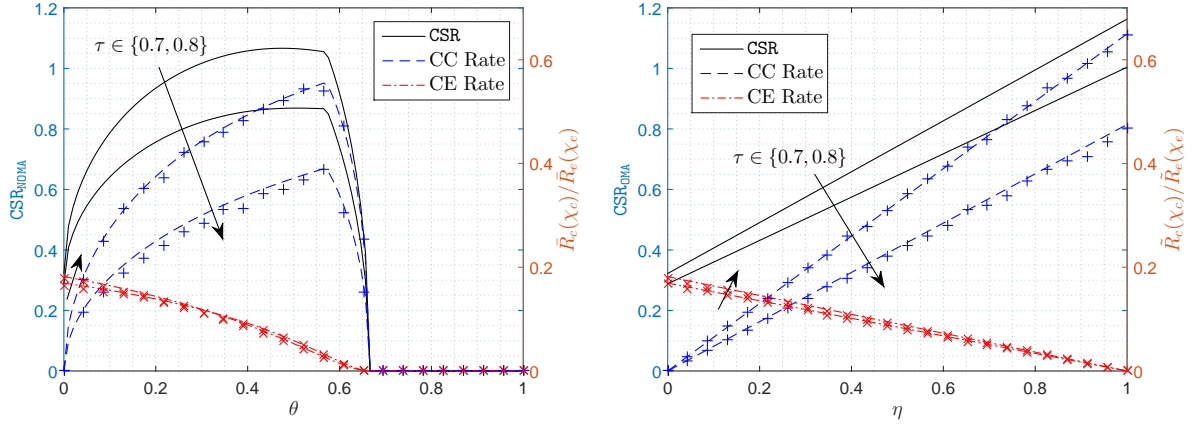


Figure 4. CSR and mean transmission rates of CC and CE users under NOMA (Left) and OMA (Right). The solid and dashed curves correspond to the analytical results and the markers correspond to the simulation results.

analytical results, whereas the markers correspond to the simulation results. The figure gives the visual verifications of the trends of transmission rate functions discussed in Section V. It can be seen that the CSR and the transmission rates are zero for $\theta > \theta_{NC} \approx 0.66$ which verifies the necessary condition for NOMA operation. In addition, we can see that the transmission rate of the CE user monotonically decreases with $\theta \leq \theta_{NC}$, whereas the transmission rate of the CC user is a monotonically increasing and decreasing function of θ for $0 < \theta \leq \hat{\theta}$ and $\hat{\theta} < \theta \leq \theta_{NC}$, respectively, where $\hat{\theta} = 0.5$ (see (41)).

Fig. 5 verifies that the transmission rate outage probabilities and upper bounds of the mean delay outage probabilities of the CC and CE users closely match with the simulation results. The outage probabilities of CC and CE users follow exactly opposite trend of their mean transmission rates, as expected. The outage probabilities of the CC user degrade with increase of τ because of two reasons: 1) increase in the mean number of CC users sharing the same RB and 2) decrease of the success probability of CC user. However, a similar direct trend is not visible for the CE user with respect to τ . This is because while increasing τ decreases the mean number of CE users, it also decreases the success probability of the typical CE user.

Now, we illustrate the transmission rate region to show the maximum achievable transmission rates of the CC and CE users with respect to each other in Fig. 6 for NOMA and OMA systems. As expected, the transmission rate region shrinks down with the increase of ν as it lowers the scheduling probabilities of both the CC and CE users. We also observe that the NOMA system

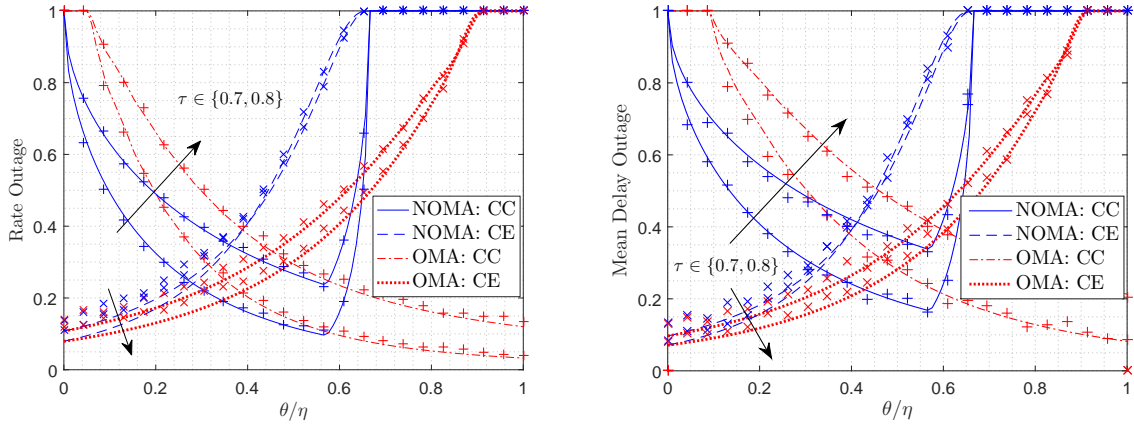


Figure 5. The outage probabilities of transmission rates (Left) and mean delays (Right) of the CC and CE users. The solid and dashed curves correspond to the analytical results and the markers correspond to the simulation results.

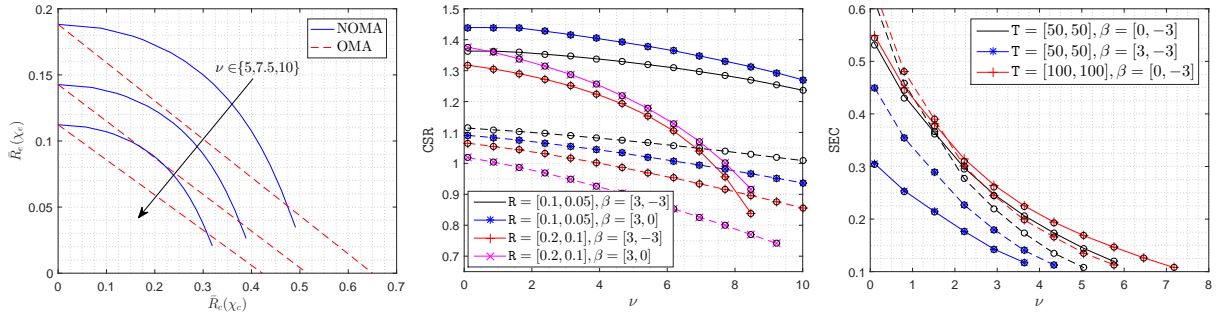


Figure 6. Rate region of the CC and CE users in NOMA and OMA for $\beta = [\beta_c, \beta_e] = [3, 0]$ in dB (Left). Maximum CSR under rate constraints where $R = [R_c, R_e]$ (Middle) and maximum SEC under minimum EC constraints (Right) for $(\theta_c, \theta_e) = (0.2, 0.2)$ and $(\varrho_c, \varrho_e) = (0.05, 0.05)$ where $T = [t_c, t_e]$. The solid and dashed lines correspond the NOMA and OMA, respectively.

outperforms the OMA system for the larger portion of the rate region. In the OMA system, the optimal time allocation with respect to the CC (CE) user is $\eta = 1$ ($\eta = 0$) which reduces the transmission rate of the CE (CC) user to zero. Unlike this, in NOMA system, the optimal power allocation with respect to the CC user is $\hat{\theta}$. Hence, at the point of the maximum achievable rate of the CC user corresponding to the power allocation $\hat{\theta}$, the CE user gets the remaining power $1 - \hat{\theta}$ which allows it to achieve non-zero transmission rate.

Fig. 6 (Middle) shows the achievable CSR with respect to ν under minimum transmission rate constraints and Fig 6 (Left) shows the achievable SEC with respect to ν under minimum EC constraints. The circular markers correspond to the proposed solution and the curves correspond to the exact optimal solution. We observe that the maximum achievable CSR and CSR drops with

the increase of ν for both NOMA and OMA systems. This is because the mean transmission rates of both CC and CE users drop with the increase of ν (due to the increase of the number of users sharing the same RB). This restricts the feasible range of θ and thus that of both CSR and SEC. The middle figure clearly depicts that the NOMA provides better CSR as compared to OMA. The CSR drops at a higher rate when the minimum required transmission rates are higher as it causes the power consumption to aggressively increase with the increase in ν . Fig. 6 (Left) depicts that the NOMA provides better SEC for lower SIR threshold at higher values of ν as compared to OMA. This is because the packet service rates of CC and CE users (thus the SEC) are predominantly determined by their scheduling probabilities for the lower values of SIR thresholds which are higher in NOMA as compared to OMA for a given ν .

VII. CONCLUSION

This paper has provided a comprehensive analysis of downlink two-user NOMA enabled cellular networks for both RT and NRT services. In particular, a new 3GPP-inspired user ranking technique has been proposed wherein the CC and CE users are paired for the non-orthogonal transmission. To the best of our knowledge, this is the first stochastic geometry-based approach to analyze downlink NOMA using a 3GPP-inspired user ranking scheme that depends upon both the link qualities from the serving and dominant interfering BSs. Unlike the ranking techniques used in the literature, the proposed technique ranks users accurately with distinct link qualities which is vital to obtain performance gains in NOMA. For the proposed user ranking, we first derive the moments and approximate distributions of the meta distributions for the CC and CE users. Next, we obtain the distributions of their transmission rates and mean delays under random scheduling which are then used to characterize CSR for NRT service and SEC for RT service, respectively. Using these results, we investigate two RA techniques with objectives to maximize CSR and SEC. The numerical results demonstrated that NOMA along with the proposed user ranking technique results in a significantly higher CSR and improved transmission rate region for the CC and CE users as compared to OMA. In addition, our results showed that NOMA provides improved SEC as compared to OMA for the higher user density. The natural extension of this work is to analyze the N -user downlink NOMA in cellular networks. Besides, one could also employ the proposed way of user partitioning to analyze the transmission schemes relying on the partition of users based on their perceived link qualities, such as SFR.

APPENDIX

A. Proof of Lemma 1

Using (8) and the definitions of Ψ_{cc} and Ψ_{ce} given in (2), it is easy to see that a uniformly distributed user in the typical cell V_o is the typical CC user if $R_o \leq \tau R_d$ and the typical CE user if $R_o > \tau R_d$. Therefore, the probability that the typical user is the CC user becomes

$$\mathbb{P}[R_o \leq R_d\tau] = (2\pi\rho\lambda)^2 \int_0^\infty \int_0^{r_d\tau} r_o r_d \exp(-\pi\rho\lambda r_d^2) dr_o dr_d = \tau^2.$$

and thus the probability that the typical user is the CE user becomes $1 - \tau^2$. Now, using Eq. (8) and $\mathbb{P}[R_o \leq R_d\tau] = \tau^2$, we obtain the CDF of R_o for the CC user as $F_{R_o}^c(r_o) =$

$$\mathbb{P}[R_o \leq r_o | R_o < R_d\tau] = \frac{(2\pi\rho\lambda)^2}{\tau^2} \int_0^{r_o} \int_{\frac{u}{\tau}}^\infty uv \exp(-\pi\rho\lambda v^2) dv du = 1 - \exp(-\pi\rho\lambda r_o^2/\tau^2), \quad (42)$$

for $r_o \geq 0$. Using $R_o \leq R_d\tau$, we obtain the CDF of R_d of CC user as

$$F_{R_d|R_o}^c(r_d | r_o) = \mathbb{P}[R_d \leq r_d | R_d > r_o/\tau] = 1 - \exp(-\pi\rho\lambda(r_d^2 - r_o^2/\tau^2)), \quad (43)$$

for $r_d \geq \frac{r_o}{\tau}$. Therefore, the joint pdf of R_o and R_d for the CC user given in (11) directly follows using the Bayes' theorem along with (42) and (43). Similarly, using (8) and $\mathbb{P}[R_o > R_d\tau] = 1 - \tau^2$, we obtain the CDF of R_o for the CE user as

$$\begin{aligned} F_{R_o}^e(r_o) &= \mathbb{P}[R_o \leq r_o | R_o > R_d\tau] = \frac{(2\pi\rho\lambda)^2}{1 - \tau^2} \int_0^{r_o} \int_u^{\frac{u}{\tau}} uv \exp(-\pi\rho\lambda v^2) dv du \\ &= 1 - \frac{\exp(-\pi\rho\lambda r_o^2)}{1 - \tau^2} [1 - \tau^2 \exp(-\pi\rho\lambda r_o^2(\tau^{-2} - 1))], \end{aligned} \quad (44)$$

for $r_o > 0$. Now, the conditional CDF of R_d given R_o for the CE user can be determined as

$$F_{R_d|R_o}^e(r_d | r_o) = \mathbb{P}\left[R_d \leq r_d | R_d < \frac{r_o}{\tau}\right] = \frac{\mathbb{P}[R_d \leq r_d]}{\mathbb{P}[R_d < \frac{r_o}{\tau}]} = \frac{1 - \exp(-\pi\rho\lambda(r_d^2 - r_o^2))}{1 - \exp(-\pi\rho\lambda r_o^2(\tau^{-2} - 1))}, \quad (45)$$

for $r_o < r_d < \frac{r_o}{\tau}$ and $F_{R_d|R_o}^e(r_d | r_o) = 1$ for $r_d \geq \frac{r_o}{\tau}$. Finally, the joint pdf of R_o and R_d for the CE given in Eq. (14) directly follows using the Bayes' theorem and Equations (44) and (45).

B. Proof of Theorem 1

The success probability of the CC user at $\mathbf{y} \in V_o$ conditioned on $\mathbf{y} = R_o$ and Φ is

$$p_c(\chi_c \mid \mathbf{y}, \Phi) = \mathbb{P}(\mathcal{E}_c \mid \mathbf{y}, \Phi) \stackrel{(a)}{=} \prod_{\mathbf{x} \in \Phi} \frac{1}{1 + R_o^\alpha \chi_c \|\mathbf{x}\|^{-\alpha}},$$

where step (a) follows from the independence of the fading gains. Let $\mathbf{x}_d = \arg \min_{\mathbf{x} \in \Phi} \|\mathbf{x}\|$ and $\tilde{\Phi} = \Phi \setminus \{\mathbf{x}_d\}$. Then, the b -th moment of conditional success probability becomes

$$\begin{aligned} M_b^c(\chi_c) &= \mathbb{E}_{R_o, \Phi} \left[\frac{1}{(1 + \chi_c(R_o/R_d)^\alpha)^b} \prod_{\mathbf{x} \in \tilde{\Phi}} \frac{1}{(1 + R_o^\alpha \chi_c \|\mathbf{x}\|^{-\alpha})^b} \right] \\ &= \mathbb{E}_{R_o, R_d} \left[\frac{1}{(1 + \chi_c(R_o/R_d)^\alpha)^b} \mathbb{E}_{\tilde{\Phi}} \left[\prod_{\mathbf{x} \in \tilde{\Phi}} \frac{1}{(1 + R_o^\alpha \chi_c \|\mathbf{x}\|^{-\alpha})^b} \mid \mathbf{x}_d \right] \right] \\ &\stackrel{(a)}{=} \mathbb{E}_{R_o, R_d} \left[\frac{1}{(1 + \chi_c(R_o/R_d)^\alpha)^b} \exp \left(-\lambda \int_{\mathbb{R}^2 \setminus \mathcal{B}_y(R_d)} [1 - (1 + R_o^\alpha \chi_c \|\mathbf{x}\|^{-\alpha})^{-b}] d\mathbf{x} \right) \right] \\ &= \mathbb{E}_{R_o, R_d} \left[\frac{1}{(1 + \chi_c(R_o/R_d)^\alpha)^b} \exp \left(-\pi \lambda R_o^2 \tilde{\mathcal{Z}}_b(\chi_c, R_o/R_d) \right) \right], \end{aligned}$$

where $\tilde{\mathcal{Z}}_b(\chi_c, a) = \chi_c^\delta \int_{\chi_c^{-\delta} a^{-2}}^\infty [1 - (1 + t^{-\frac{1}{\delta}})^{-b}] dt$, and step (a) follows by approximating $\tilde{\Phi}$ with the homogeneous PPP with density λ outside of the disk $\mathcal{B}_y(R_d)$ and the probability generating functional (PGFL) of the PPP. Now, using the joint pdf of R_o and R_d for the CC user given in (11), we get

$$\begin{aligned} M_b^c(\chi_c) &= \frac{(2\pi\rho\lambda)^2}{\tau^2} \int_0^\infty r_d \exp(-\pi\rho\lambda r_d^2) \int_0^{\tau r_d} \frac{\exp \left(-\pi\lambda r_o^2 \tilde{\mathcal{Z}}_b(\chi_c, r_o/r_d) \right)}{(1 + \chi_c(r_o/r_d)^\alpha)^b} r_o dr_o dr_d \\ &\stackrel{(a)}{=} \frac{2(\pi\rho\lambda)^2}{\tau^2} \int_0^{\tau^2} \frac{1}{(1 + \chi_c v^{\frac{1}{\delta}})^b} \int_0^\infty r_d^3 \exp \left(-\pi\lambda r_d^2 [\rho + \tilde{\mathcal{Z}}_b(\chi_c, v^{\frac{1}{2}})] \right) dr_d dv, \end{aligned}$$

where step (a) follows using the substitution $(r_o/r_d)^\alpha = v^{\frac{1}{\delta}}$ and the exchange of the integral orders. Further, solving the inner integral gives $M_b^c(\chi_c)$ as in (17) such that $\mathcal{Z}(\chi_c, v) = \tilde{\mathcal{Z}}(\chi_c, v^{\frac{1}{2}})$. Following similar steps and using the joint pdf of R_o and R_d given in (14), the b -th moment of the conditional success probability for the CE user can be obtained as

$$M_b^e(\chi_e) = \frac{(2\pi\rho\lambda)^2}{1 - \tau^2} \int_0^\infty r_d \exp(-\pi\rho\lambda r_d^2) \int_{\tau r_d}^{r_d} \frac{\exp \left(-\pi\lambda r_o^2 \tilde{\mathcal{Z}}_b(\chi_e, r_o/r_d) \right)}{(1 + \chi_e(r_o/r_d)^\alpha)^b} r_o dr_o dr_d$$

$$= \frac{2(\pi\rho\lambda)^2}{1-\tau^2} \int_{\tau^2}^1 \frac{1}{(1+\chi_e v^{\frac{1}{\delta}})^b} \int_0^\infty r_d^3 \exp\left(-\pi\lambda r_d^2 \left[\rho + v\tilde{\mathcal{Z}}_b\left(\chi_e, v^{\frac{1}{2}}\right)\right]\right) dr_d dv,$$

Finally, solving the inner integral gives $M_b^e(\chi_e)$ as in (17) where $\mathcal{Z}(\chi_e, v) = \tilde{\mathcal{Z}}(\chi_e, v^{\frac{1}{2}})$.

C. Proof of Lemma 2

The n -th moment of the area of a random set $A \subset \mathbb{R}^2$ can be obtained as [52]

$$\mathbb{E}[|A|^n] = \int_{\mathbb{R}^d} \cdots \int_{\mathbb{R}^d} \mathbb{P}[\mathbf{x}_1, \dots, \mathbf{x}_n \in A] d\mathbf{x}_1 \dots d\mathbf{x}_n. \quad (46)$$

Let $\mathcal{B}_{\mathbf{x}}$ and $\tilde{\mathcal{B}}_{\mathbf{x}}$ be the disks of radii r and $r\tau^{-1}$ both centered at $\mathbf{x} \equiv (r, \theta)$ and let $\mathcal{A}_{\mathbf{x}}$ be the annulus formed by the two disks $\tilde{\mathcal{B}}_{\mathbf{x}}$ and $\mathcal{B}_{\mathbf{x}}$. By definition, the point \mathbf{x} belongs to V_{oc} only if $\Phi(\mathcal{B}_{\mathbf{x}}) = 0$ (i.e., $\mathbf{x} \in V_o$) and $\Phi(\mathcal{A}_{\mathbf{x}}) = 0$. Thus, we have $\mathbb{P}[\mathbf{x} \in V_{oc}] =$

$$\mathbb{P}[\mathbf{x} \in V_{oc} \mid \mathbf{x} \in V_o] \mathbb{P}[\mathbf{x} \in V_o] \stackrel{(a)}{=} \exp(-\lambda|\mathcal{A}_{\mathbf{x}}|) \exp(-\lambda|\mathcal{B}_{\mathbf{x}}|) = \exp(-\lambda|\tilde{\mathcal{B}}_{\mathbf{x}}|), \quad (47)$$

where step (a) follows from the independence property and the *void probability* of the PPP. However, the point \mathbf{x} belongs to V_{oe} only if $\Phi(\mathcal{B}_{\mathbf{x}}) = 0$ and $\Phi(\mathcal{A}_{\mathbf{x}}) \neq 0$. Thus, we have

$$\begin{aligned} \mathbb{P}[\mathbf{x} \in V_{oe}] &= \mathbb{P}[\mathbf{x} \in V_{oe} \mid \mathbf{x} \in V_o] \mathbb{P}[\mathbf{x} \in V_o] \\ &\stackrel{(a)}{=} [1 - \exp(-\lambda|\mathcal{A}_{\mathbf{x}}|)] \exp(-\lambda|\mathcal{B}_{\mathbf{x}}|) = \exp(-\lambda|\mathcal{B}_{\mathbf{x}}|) - \exp(-\lambda|\tilde{\mathcal{B}}_{\mathbf{x}}|), \end{aligned} \quad (48)$$

where step (a) follows from the independence property and the *void probability* of the PPP. Thus, using (46), (47) and (48), we get the mean areas of the CC and CE regions as in (21).

Similarly, the probability of $\{\mathbf{x}_1, \mathbf{x}_2\} \in V_{oc}$ can be directly determined as $\mathbb{P}[\mathbf{x}_1, \mathbf{x}_2 \in V_{oc}] = \exp(-\lambda|\mathcal{C}_3|)$, where $\mathcal{C}_3 = \tilde{\mathcal{B}}_{\mathbf{x}_1} \cup \tilde{\mathcal{B}}_{\mathbf{x}_2}$. Thus, using this and (46), we can easily obtain the second moment of the area of the CC region as in (22). On the other hand, to evaluate the second moment of area of the CE region we require the probability of $\{\mathbf{x}_1, \mathbf{x}_2\} \in V_{oe}$ which requires a careful consideration of the intersection of various sets of two disks. Let $d = \|\mathbf{x}_1 - \mathbf{x}_2\| = (r_1^2 + r_2^2 - 2r_1r_2 \cos(\theta_1 - \theta_2))^{\frac{1}{2}}$. Consider the two cases as shown in Fig. 7 such that Case 1 occurs if $d \leq \tau^{-1}|r_1 - r_2|$, while the Case 2 occurs otherwise. Now, we derive $\mathbb{P}[\mathbf{x}_1, \mathbf{x}_2 \in V_{oe}]$ for these cases in the following.

Case 1: In this case, $\{\mathbf{x}_1, \mathbf{x}_2\} \in V_{oe}$ if $\Phi(\mathcal{C}_o) = 0$ (i.e. $\{\mathbf{x}_1, \mathbf{x}_2\} \in V_o$) and if

$$\Phi(\mathcal{C}_2 \setminus \mathcal{C}_o) \neq 0 \text{ for } r_2 \leq r_1 \text{ or } \Phi(\mathcal{C}_1 \setminus \mathcal{C}_o) \neq 0 \text{ for } r_1 < r_2,$$

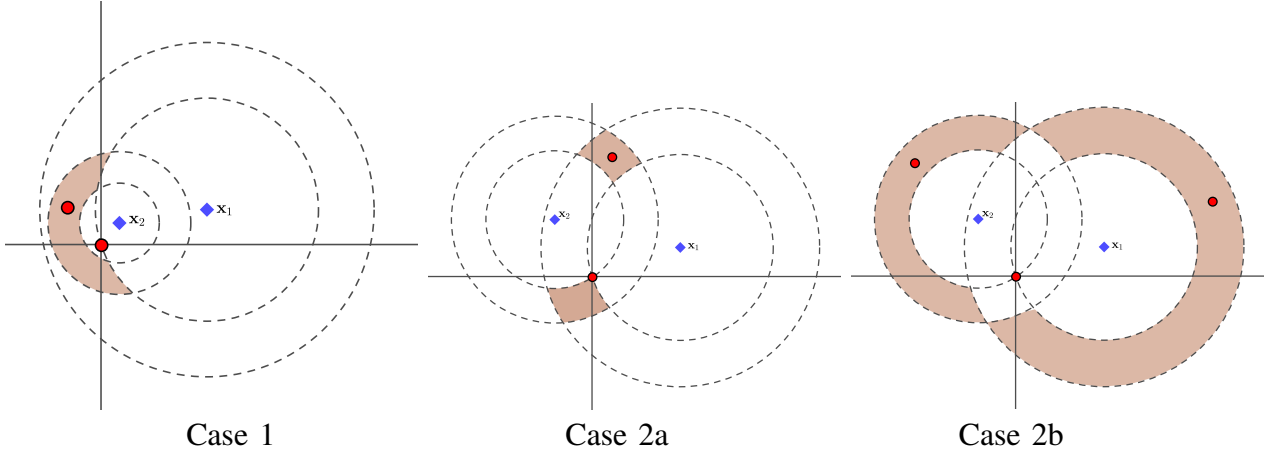


Figure 7. Illustration of the cases when $\{\mathbf{x}_1, \mathbf{x}_2\} \in V_{oe}$ given $\{\mathbf{x}_1, \mathbf{x}_2\} \in V_o$ (i.e. $\Phi(\mathcal{C}_o) = 0$). The blue diamonds represent the locations $\{\mathbf{x}_1, \mathbf{x}_2\}$, whereas the red dots represent the locations of serving and dominant BSs.

where $\mathcal{C}_o = \mathcal{B}_{\mathbf{x}_1} \cup \mathcal{B}_{\mathbf{x}_2}$, $\mathcal{C}_1 = \tilde{\mathcal{B}}_{\mathbf{x}_1} \cup \mathcal{B}_{\mathbf{x}_2}$ and $\mathcal{C}_2 = \mathcal{B}_{\mathbf{x}_1} \cup \tilde{\mathcal{B}}_{\mathbf{x}_2}$. Fig. 7 (Left) depicts the second condition of this case for $r_2 \leq r_1$. Thus, we have

$$\mathbb{P}[\mathbf{x}_1, \mathbf{x}_2 \in V_o] = \exp(-\lambda|\mathcal{C}_o|) \quad (49)$$

$$\mathbb{P}[\mathbf{x}_1, \mathbf{x}_2 \in V_{oe} \mid \mathbf{x}_1, \mathbf{x}_2 \in V_o] = \exp(-\lambda(|\mathcal{C}_1| - |\mathcal{C}_o|)) \mathbb{1}_{r_1 \leq r_2} + \exp(-\lambda(|\mathcal{C}_2| - |\mathcal{C}_o|)) \mathbb{1}_{r_2 < r_1}. \quad (50)$$

Therefore, using (49) and (50) and the independence property of the PPP, we obtain

$$\mathbb{P}[\mathbf{x}_1, \mathbf{x}_2 \in V_{oe}] = \exp(-\lambda|\mathcal{C}_1|) \mathbb{1}_{r_1 \leq r_2} + \exp(-\lambda|\mathcal{C}_2|) \mathbb{1}_{r_2 < r_1}. \quad (51)$$

Case 2: In this case, $\{\mathbf{x}_1, \mathbf{x}_2\} \in V_{oe}$ if $\Phi(\mathcal{C}_o) = 0$ and if one of the following conditions is met:

2a) $\Phi(\mathcal{A}_o) \neq 0$, and 2b) $\Phi(\mathcal{C}_3 \setminus \mathcal{C}_1) \neq 0$, and $\Phi(\mathcal{C}_3 \setminus \mathcal{C}_2) \neq 0$,

where $\mathcal{A}_o = \mathcal{A}_{\mathbf{x}_1} \cap \mathcal{A}_{\mathbf{x}_2}$. The above two cases are depicted in Fig. 7 (Middle and Right). Thus, we have $\mathbb{P}[\mathbf{x}_1, \mathbf{x}_2 \in V_{oe} \mid \mathbf{x}_1, \mathbf{x}_2 \in V_o] =$

$$[1 - \exp(-\lambda|\mathcal{A}_o|)] + \exp(-\lambda|\mathcal{A}_o|)[1 - \exp(-\lambda|\mathcal{C}_3 \setminus \mathcal{C}_1|)][1 - \exp(-\lambda|\mathcal{C}_3 \setminus \mathcal{C}_2|)] \quad (52)$$

We have $|\mathcal{A}_o| + |\mathcal{C}_o| = |\mathcal{C}_1| + |\mathcal{C}_2| - |\mathcal{C}_3|$. Therefore, using (49) and (52) and the independence property of the PPP, we obtain

$$\mathbb{P}[\mathbf{x}_1, \mathbf{x}_2 \in V_{oe}] = [\exp(-\lambda|\mathcal{C}_o|) - \exp(-\lambda(|\mathcal{C}_1| + |\mathcal{C}_2| - |\mathcal{C}_3|))]$$

$$+ [\exp(-\lambda(|\mathcal{C}_2| - |\mathcal{C}_3|)) - 1][\exp(-\lambda|\mathcal{C}_1|) - \exp(-\lambda|\mathcal{C}_3|)]. \quad (53)$$

Now, we derive the areas of \mathcal{C}_o , \mathcal{C}_1 , \mathcal{C}_2 , and \mathcal{C}_3 . Let $U(z_1, z_2, u)$ be the area of the union of two circles of radii z_1 and z_2 with the angular separation of u between their centers w.r.t. their intersection points. Thus, $U(z_1, z_2, u)$ can be easily obtained as given in Lemma 2. Without loss of generality, we set $\theta_2 = 0$ and $0 \leq \theta_1 < \pi$. The two disks in \mathcal{C}_o , \mathcal{C}_1 , \mathcal{C}_2 and \mathcal{C}_3 intersect (if they interest at all) at angles $u_o = \theta_1$, $u_1 = \arccos\left((\tau^{-1} - \tau)\frac{r_1}{2r_2} + \tau \cos(\theta_1)\right)$, $u_2 = \arccos\left((\tau^{-1} - \tau)\frac{r_2}{2r_1} + \tau \cos(\theta_1)\right)$ and $u_3 = \arccos\left((1 - \tau^2)\frac{r_1^2 + r_2^2}{2r_1r_2} + \tau^2 \cos(\theta_1)\right)$, respectively. The evaluation of $|\mathcal{C}_3|$ is required only for Case 2 wherein $\tilde{\mathcal{B}}_{\mathbf{x}_1}$ and $\tilde{\mathcal{B}}_{\mathbf{x}_2}$ always intersect. Thus, by definition, we have $|\mathcal{C}_o| = U(r_1, r_2, u_o)$ and $|\mathcal{C}_3| = U(r_1\tau^{-1}, r_2\tau^{-1}, u_3)$. However, $\tilde{\mathcal{B}}_{\mathbf{x}_1}$ and $\mathcal{B}_{\mathbf{x}_2}$ ($\mathcal{B}_{\mathbf{x}_1}$ and $\tilde{\mathcal{B}}_{\mathbf{x}_2}$) intersect only if $\frac{r_1}{\tau} < d + r_2$ ($\frac{r_2}{\tau} < d + r_1$), otherwise $\mathcal{B}_{\mathbf{x}_2} \subset \tilde{\mathcal{B}}_{\mathbf{x}_1}$ ($\mathcal{B}_{\mathbf{x}_1} \subset \tilde{\mathcal{B}}_{\mathbf{x}_2}$). Thus, we get

$$|\mathcal{C}_1| = \begin{cases} U(r_1\tau^{-1}, r_2, u_1), & \text{if } r_1\tau^{-1} < d + r_2, \\ \pi r_1^2 \tau^{-2}, & \text{otherwise,} \end{cases} \quad \text{and} \quad |\mathcal{C}_2| = \begin{cases} U(r_1, r_2\tau^{-1}, u_2), & \text{if } r_2\tau^{-1} < d + r_1, \\ \pi r_2^2 \tau^{-2}, & \text{otherwise.} \end{cases}$$

Finally, substituting above expressions in (51) and (53), and then integrating (51) over domain $\{d \leq \tau^{-1}|r_1 - r_2|\}$ (i.e., Case 1) and (53) over domain $\{d > \tau^{-1}|r_1 - r_2|\}$ (i.e., Case 2), we get the second moment of the area of the CE region as in (22).

D. Proof of Theorem 2

We first derive the mean transmission rate of the typical CC user at $\mathbf{y} \sim U(V_o)$ as below

$$\begin{aligned} \bar{R}_c(\chi_c) &= \mathbb{E}_{\mathbf{y}, \Phi} \left[\frac{1}{N_{oc}} \log_2(1 + \beta_c) \mathbb{E} [\mathbb{1}_{\mathcal{E}_c}(\text{SIR}_{cc}, \text{SIR}_{ce}) \mid \mathbf{y}, \Phi] \right] \\ &\stackrel{(a)}{=} \log_2(1 + \beta_c) \mathbb{E}_{|V_{oc}|} \left[\sum_{n=1}^{\infty} \frac{1}{n} \mathbb{P}(N_{oc} = n \mid |V_{oc}|) \right] \mathbb{E}_{\mathbf{y}, \Phi} [p_c(\beta_c, \beta_e \mid \mathbf{y}, \Phi)] \\ &= \log_2(1 + \beta_c) \sum_{n=1}^{\infty} \frac{1}{n} \mathbb{P}(N_{oc} = n) \mathbb{E}_{\mathbf{y}, \Phi} [p_c(\beta_c, \beta_e \mid \mathbf{y}, \Phi)], \end{aligned}$$

where step (a) follows using Assumption 1. From the definition of the meta distribution, we have $\mathbb{E}_{\mathbf{y}, \Phi} [p_c(\beta_c, \beta_e \mid \Phi)] = M_1^c(\chi_c, 1)$ for $q_c = q_e = 1$. Hence, using the distribution of CC load given in (24), we obtained $\bar{R}_c(\chi_c)$ as in (27). Similarly, using the distribution of CE load given in (25), we obtained the mean transmission rate $\bar{R}_e(\chi_e)$ of the typical CE user as in (27). Now,

we obtain the distribution of the conditional transmission rate of the typical CC user as

$$\begin{aligned}
\mathcal{R}_c(\mathbf{r}_c; \chi_c) &= \mathbb{P} [p_c(\beta_c, \beta_e | \mathbf{y}, \Phi) \leq \mathbf{r}_c N_{oc} \log_2(1 + \beta_c)^{-1}] \\
&\stackrel{(a)}{=} \mathbb{E}_{N_{oc}} [\mathbb{P} [p_c(\beta_c, \beta_e | \mathbf{y}, \Phi) \leq \mathbf{r}_c N_{oc} \log_2(1 + \beta_c)^{-1} | N_{oc}]] \\
&\stackrel{(b)}{=} \mathbb{E}_{N_{oc}} [I (\min (\mathbf{r}_c N_{oc} \log_2(1 + \beta_c)^{-1}, 1); \kappa_{1c}, \kappa_{2c})]
\end{aligned}$$

where step (a) follows using Assumption 1, and step (b) follows using the beta approximation of the meta distribution of the success probability (see (20)). Similarly, we obtain the distribution of the conditional transmission rate of the typical CE user as in (29).

REFERENCES

- [1] P. D. Mankar and H. S. Dhillon, “Meta distribution for downlink NOMA in cellular networks with 3GPP-inspired user ranking,” *IEEE Globecom*, Dec. 2019. [Online]. Available: <https://arxiv.org/abs/1905.00726>
- [2] Z. Ding, X. Lei, G. K. Karagiannidis, R. Schober, J. Yuan, and V. K. Bhargava, “A survey on non-orthogonal multiple access for 5G networks: Research challenges and future trends,” *IEEE J. Sel. Areas Commun.*, vol. 35, no. 10, pp. 2181–2195, Oct. 2017.
- [3] Z. Ding, Z. Yang, P. Fan, and H. V. Poor, “On the performance of non-orthogonal multiple access in 5G systems with randomly deployed users,” *IEEE Signal Process. Lett.*, vol. 21, no. 12, pp. 1501–1505, Dec. 2014.
- [4] Z. Ding, P. Fan, and H. V. Poor, “Impact of user pairing on 5G non-orthogonal multiple-access downlink transmissions,” *IEEE Trans. Veh. Technol.*, vol. 65, no. 8, pp. 6010–6023, Aug. 2016.
- [5] J. Choi, “Power allocation for max-sum rate and max-min rate proportional fairness in noma,” *IEEE Commun. Lett.*, vol. 20, no. 10, pp. 2055–2058, 2016.
- [6] Y. Liu, Z. Ding, M. Elkashlan, and H. V. Poor, “Cooperative non-orthogonal multiple access with simultaneous wireless information and power transfer,” *IEEE J. Sel. Areas Commun.*, vol. 34, no. 4, pp. 938–953, April 2016.
- [7] Z. Ding, M. Peng, and H. V. Poor, “Cooperative non-orthogonal multiple access in 5G systems,” *IEEE Communications Letters*, vol. 19, no. 8, pp. 1462–1465, Aug. 2015.
- [8] S. Timotheou and I. Krikidis, “Fairness for non-orthogonal multiple access in 5G systems,” *IEEE Signal Process. Lett.*, vol. 22, no. 10, pp. 1647–1651, Oct. 2015.
- [9] J. Zhu, J. Wang, Y. Huang, S. He, X. You, and L. Yang, “On optimal power allocation for downlink non-orthogonal multiple access systems,” *IEEE J. Sel. Areas Commun.*, vol. 35, no. 12, pp. 2744–2757, 2017.
- [10] K. S. Ali, H. Elsawy, A. Chaaban, and M.-S. Alouini, “Non-orthogonal multiple access for large-scale 5G networks: Interference aware design,” *IEEE Access*, vol. 5, pp. 21 204–21 216, 2017.
- [11] M. Haenggi, *Stochastic geometry for wireless networks*. Cambridge University Press, 2012.
- [12] J. G. Andrews, A. K. Gupta, and H. S. Dhillon, “A primer on cellular network analysis using stochastic geometry,” *arXiv:1604.03183*.
- [13] B. Blaszczyszyn, M. Haenggi, P. Keeler, and S. Mukherjee, *Stochastic Geometry Analysis of Cellular Networks*. Cambridge University Press, 2018.

- [14] K. S. Ali, M. Haenggi, H. ElSawy, A. Chaaban, and M.-S. Alouini, "Downlink non-orthogonal multiple access (NOMA) in Poisson networks," *IEEE Trans. Commun.*, vol. 67, no. 2, pp. 1613–1628, Feb. 2019.
- [15] K. Ali, H. Elsawy, and M. Alouini, "Meta distribution of downlink non-orthogonal multiple access (NOMA) in Poisson networks," *IEEE Wireless Commun. Lett.*, vol. 8, no. 2, pp. 572–575, April 2019.
- [16] M. Salehi, H. Tabassum, and E. Hossain, "Meta distribution of SIR in large-scale uplink and downlink NOMA networks," *IEEE Trans. Commun.*, vol. 67, no. 4, pp. 3009–3025, April 2019.
- [17] ———, "Accuracy of distance-based ranking of users in the analysis of NOMA systems," *IEEE Trans. Commun.*, vol. 67, no. 7, pp. 5069 – 5083, July 2019.
- [18] H. Tabassum, E. Hossain, and J. Hossain, "Modeling and analysis of uplink non-orthogonal multiple access in large-scale cellular networks using Poisson cluster processes," *IEEE Trans. Commun.*, vol. 65, no. 8, pp. 3555–3570, Aug. 2017.
- [19] M. Haenggi, "The meta distribution of the SIR in Poisson bipolar and cellular networks," *IEEE Trans. Wireless Commun.*, vol. 15, no. 4, pp. 2577–2589, April 2016.
- [20] Y. Liu, Z. Qin, M. Elkashlan, A. Nallanathan, and J. A. McCann, "Non-orthogonal multiple access in large-scale heterogeneous networks," *IEEE J. Sel. Areas Commun.*, vol. 35, no. 12, pp. 2667–2680, Dec. 2017.
- [21] Z. Zhang, H. Sun, and R. Q. Hu, "Downlink and uplink non-orthogonal multiple access in a dense wireless network," *IEEE J. Sel. Areas Commun.*, vol. 35, no. 12, pp. 2771–2784, Dec. 2017.
- [22] F. Dominique, C. G. Gerlach, N. Gopalakrishnan, A. Rao, J. P. Seymour, R. Soni, A. Stolyar, H. Viswanathan, C. Weaver, and A. Weber, "Self-organizing interference management for LTE," *Bell Labs Tech. J.*, vol. 15, no. 3, pp. 19–42, 2010.
- [23] M. Wildemeersch, T. Q. Quek, M. Kountouris, A. Rabbachin, and C. H. Slump, "Successive interference cancellation in heterogeneous networks," *IEEE Trans. Commun.*, vol. 62, no. 12, pp. 4440–4453, Dec. 2014.
- [24] V. V. Chetlur and H. S. Dhillon, "Downlink coverage analysis for a finite 3-D wireless network of unmanned aerial vehicles," *IEEE Trans. Commun.*, vol. 65, no. 10, pp. 4543–4558, Oct. 2017.
- [25] J. Choi, "Power allocation for max-sum rate and max-min rate proportional fairness in NOMA," *IEEE Commun. Lett.*, vol. 20, no. 10, pp. 2055–2058, Oct. 2016.
- [26] Y. Sun, D. W. K. Ng, Z. Ding, and R. Schober, "Optimal joint power and subcarrier allocation for full-duplex multicarrier non-orthogonal multiple access systems," *IEEE Trans. Commun.*, vol. 65, no. 3, pp. 1077–1091, March 2017.
- [27] P. Parida and S. S. Das, "Power allocation in OFDM based NOMA systems: A DC programming approach," in *IEEE Globecom Workshops*, Dec. 2014, pp. 1026–1031.
- [28] C. Wang, J. Chen, and Y. Chen, "Power allocation for a downlink non-orthogonal multiple access system," *IEEE Wireless Commun. Lett.*, vol. 5, no. 5, pp. 532–535, Oct 2016.
- [29] Y. Zhang, H. Wang, T. Zheng, and Q. Yang, "Energy-efficient transmission design in non-orthogonal multiple access," *IEEE Trans. Veh. Technol.*, vol. 66, no. 3, pp. 2852–2857, March 2017.
- [30] F. Fang, H. Zhang, J. Cheng, and V. C. Leung, "Energy-efficient resource allocation for downlink non-orthogonal multiple access network," *IEEE Trans. Commun.*, vol. 64, no. 9, pp. 3722–3732, Sept. 2016.
- [31] Z. Chen, Z. Ding, X. Dai, and R. Zhang, "An optimization perspective of the superiority of NOMA compared to conventional OMA," *IEEE Trans. Signal Process.*, vol. 65, no. 19, pp. 5191–5202, Oct. 2017.
- [32] D. Wu and R. Negi, "Effective capacity: a wireless link model for support of quality of service," *IEEE Trans. Wireless Commun.*, vol. 2, no. 4, pp. 630–643, July 2003.
- [33] W. Yu, L. Musavian, and Q. Ni, "Link-layer capacity of NOMA under statistical delay QoS guarantees," *IEEE Trans. Commun.*, vol. 66, no. 10, pp. 4907–4922, Oct. 2018.

- [34] C. Xiao, J. Zeng, W. Ni, X. Su, R. P. Liu, T. Lv, and J. Wang, "Downlink MIMO-NOMA for ultra-reliable low-latency communications," *IEEE J. Sel. Areas Commun.*, vol. 37, no. 4, pp. 780–794, April 2019.
- [35] J. Choi, "Effective capacity of NOMA and a suboptimal power control policy with delay QoS," *IEEE Trans. Commun.*, vol. 65, no. 4, pp. 1849–1858, April 2017.
- [36] D. Qiao, M. C. Gursoy, and S. Velipasalar, "Transmission strategies in multiple-access fading channels with statistical QoS constraints," *IEEE Trans. Inf. Theory*, vol. 58, no. 3, pp. 1578–1593, March 2012.
- [37] S. Schiessl, M. Skoglund, and J. Gross, "NOMA in the uplink: Delay analysis with imperfect CSI and finite-length coding," *arxiv:1903.09586*.
- [38] P. Parida and H. S. Dhillon, "Stochastic geometry-based uplink analysis of massive MIMO systems with fractional pilot reuse," *IEEE Trans. Wireless Commun.*, vol. 18, no. 3, pp. 1651–1668, March 2019.
- [39] M. Haenggi, "User point processes in cellular networks," *IEEE Wireless Commun. Lett.*, vol. 6, no. 2, pp. 258–261, April 2017.
- [40] M. Afshang and H. S. Dhillon, "Poisson cluster process based analysis of hetnets with correlated user and base station locations," *IEEE Trans. Wireless Commun.*, vol. 17, no. 4, pp. 2417–2431, April 2018.
- [41] P. D. Mankar, G. Das, and S. S. Pathak, "Modeling and coverage analysis of BS-centric clustered users in a random wireless network," *IEEE Wireless Commun. Lett.*, vol. 5, no. 2, pp. 208–211, April 2016.
- [42] R. R. Rao and A. Ephremides, "On the stability of interacting queues in a multiple-access system," *IEEE Trans. Inf. Theory*, vol. 34, no. 5, pp. 918–930, Sep. 1988.
- [43] T. Bonald, S. Borst, N. Hegde, and A. Proutière, *Wireless data performance in multi-cell scenarios*. ACM, 2004.
- [44] Y. Zhong, M. Haenggi, T. Q. S. Quek, and W. Zhang, "On the stability of static Poisson networks under random access," *IEEE Trans. on Commun.*, vol. 64, no. 7, pp. 2985–2998, July 2016.
- [45] Y. Zhong, T. Q. S. Quek, and X. Ge, "Heterogeneous cellular networks with spatio-temporal traffic: Delay analysis and scheduling," *IEEE J. Sel. Areas Commun.*, vol. 35, no. 6, pp. 1373–1386, June 2017.
- [46] B. Bllaszcyszyn, R. Ibrahim, and M. K. Karray, "Spatial disparity of QoS metrics between base stations in wireless cellular networks," *IEEE Trans. on Commun.*, vol. 64, no. 10, pp. 4381–4393, Oct. 2016.
- [47] P. D. Mankar, P. Parida, H. S. Dhillon, and M. Haenggi, "Distance from nucleus to uniformly random point in the typical and the Crofton cells of the Poisson-Voronoi tessellation," *arXiv:1907.03635*.
- [48] Y. Wang, M. Haenggi, and Z. Tan, "The meta distribution of the SIR for cellular networks with power control," *IEEE Trans. Commun.*, vol. 66, no. 4, pp. 1745–1757, April 2018.
- [49] J. Gil-Pelaez, "Note on the inversion theorem," *Biometrika*, vol. 38, no. 3-4, pp. 481–482, Dec. 1951.
- [50] M. Tanemura, "Statistical distributions of Poisson Voronoi cells in two and three dimensions," *Forma*, vol. 18, no. 4, p. 221247, 2003.
- [51] I. Atencia and P. Moreno, "A discrete-time Geo/G/1 retrial queue with general retrial times," *Queueing systems*, vol. 48, no. 1-2, pp. 5–21, Sept. 2004.
- [52] H. E. Robbins, "On the measure of a random set," *Ann. Math. Statist.*, vol. 15, no. 1, pp. 70–74, March 1944.